HHS Public Access

Author manuscript

Dev Cell. Author manuscript; available in PMC 2022 September 27.

Published in final edited form as:

Dev Cell. 2021 September 27; 56(18): 2547–2561.e8. doi:10.1016/j.devcel.2021.08.006.

UV-induced reduction in Polycomb repression promotes epidermal pigmentation

Meng-Yen Li[1], **Pooja Flora**[1], **Hong Pu**[2], **Carmit Bar**[1], **Jose Silva**[3], **Idan Cohen**[4], **Phillip M. Galbo Jr.**[5], **Hequn Liu**[5,10], **Xufen Yu**[6], **Jian Jin**[6], **Haruhiko Koseki**[7,8], **John A. D'Orazio**[2], **Deyou Zheng**[5,9], **Elena Ezhkova**[1,11,*]

[1]Black Family Stem Cell Institute, Department of Cell, Developmental, and Regenerative Biology, Icahn School of Medicine at Mount Sinai, 1 Gustave L. Levy Place, New York, NY 10029, USA

[2]The Markey Cancer Center, Department of Toxicology and Cancer Biology, Department of Pediatrics, University of Kentucky College of Medicine, Lexington, KY 40506, USA

[3]Department of Pathology, Icahn School of Medicine at Mount Sinai, 1425 Madison Avenue, New York, NY 10029, USA

[4]The Shraga Segal Department of Microbiology, Immunology and Genetics, Faculty of Health Science, Ben-Gurion University of the Negev, Beer Sheva 84105, Israel

[5]Department of Genetics, Albert Einstein College of Medicine, 1300 Morris Park Avenue, Bronx, NY 10461, USA

[6]Mount Sinai Center for Therapeutics Discovery, Departments of Pharmacological Sciences and Oncological Sciences, Tisch Cancer Institute, Icahn School of Medicine at Mount Sinai, New York, NY 10029, USA

[7]Laboratory for Developmental Genetics, RIKEN Center for Integrative Medical Sciences (RIKEN-IMS) 1-7-22 Suehiro-cho, Tsurumi-ku, Yokohama, 230-0045, Japan

[8]AMED-CREST, 1-7-22 Suehiro-cho Tsurumi-ku, Yokohama, 230-0045, Japan

[9]Departments of Genetics, Neurology, and Neuroscience, Albert Einstein College of Medicine, 1300 Morris Park Avenue, Bronx, NY 10461, USA

[10]Current address: Institut National de la Santé et de la Recherche Mécale (INSERM), U1036, 38000 Grenoble, France

[11]Lead Contact

[*]Correspondence should be addressed to Elena Ezhkova, PhD, Icahn School of Medicine at Mount Sinai, 1428 Madison Avenue, Atran 7–10B, New York, NY 10029, Tel: (212) 241-7184, elena.ezhkova@mssm.edu.

AUTHOR CONTRIBUTIONS

M-Y.L. and E.E. conceived and designed the experiments. M-Y.L., P.F., and I.C. performed the experiments. M-Y.L., E.E., H.L., P.G., and D.Z. performed the bioinformatic analyses. H.K. provided the *Ring1a*-null and *Ring1b-floxed* mice. J.S. provided the lentiviral overexpression constructs. W.A.B. provided the *Ring1b* I53A mice. M-Y.L., P.G., C.B., I.C., J.S., D.Z., and E.E. analyzed the data. H.P. and J.d'O. performed UVB irradiation experiments on mice and provided skins. M-Y.L., P.F., and E.E. wrote the manuscript with input from all other authors.

SUMMARY

Ultraviolet (UV) radiation is a prime environmental stressor that our epidermis is exposed to on a daily basis. To avert UV-induced damage, epidermal stem cells (EpSCs) become pigmented via a process of heterotypic interaction between melanocytes and EpSCs, however the molecular mechanisms of this interaction are not well understood. In this study we show that the function of a key chromatin regulator, the Polycomb complex, was reduced upon UV exposure in human and mouse epidermis. Genetic ablation of key Polycomb subunits in murine EpSCs, mimicking depletion upon UV exposure, results in an increased number of epidermal melanocytes and subsequent epidermal pigmentation. Genome-wide transcriptional and chromatin studies show that Polycomb regulates the expression of UV-responsive genes and identify type II collagen (COL2A1) as a critical secreted regulator of melanogenesis and epidermal pigmentation. Altogether, our findings show how UV-exposure induces Polycomb-mediated changes in EpSCs to affect melanocyte behavior and promote epidermal pigmentation.

In brief

Li et al. demonstrate that low-dose UVB exposure leads to a drastic reduction in Polycomb levels in the epidermis. Furthermore, ablation of Polycomb function in the epidermis results in epidermal pigmentation via a p53-independent pathway. They identify Polycomb-regulated protein, type II collagen, as a critical regulator of melanogenesis.

Graphical Abstract

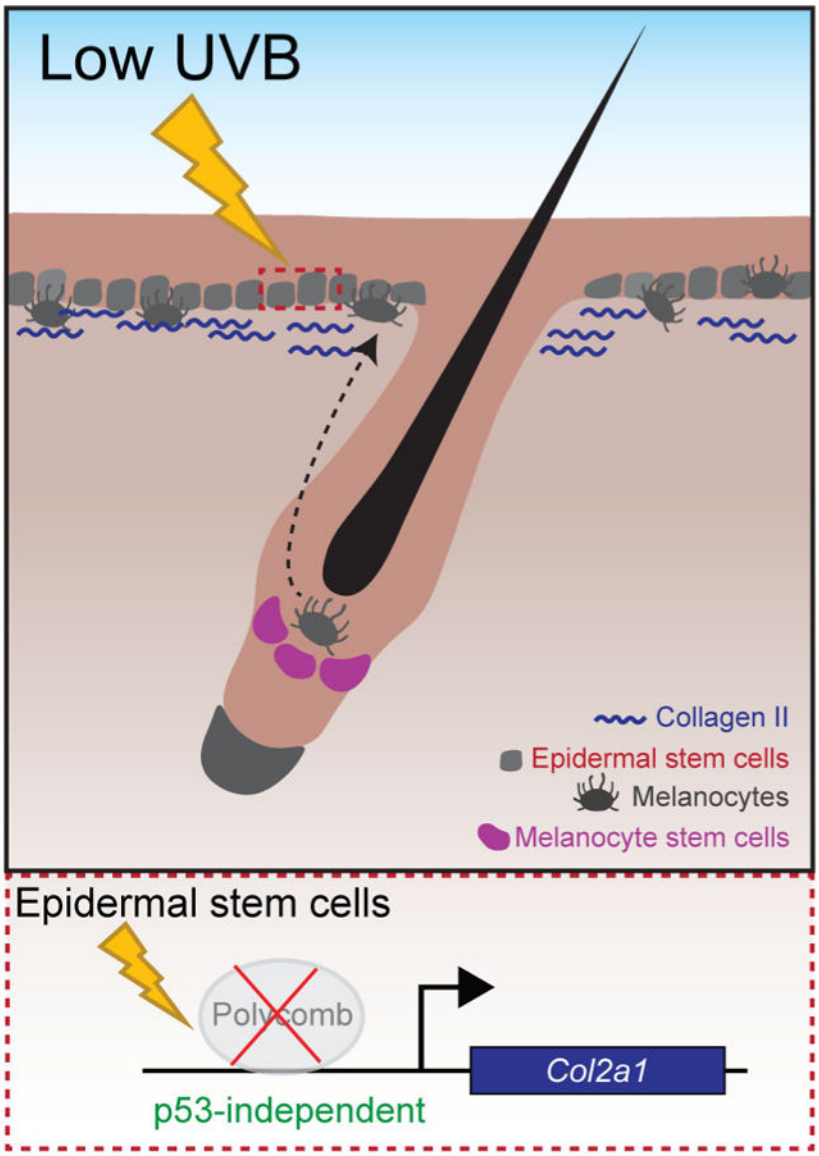

Keywords

Polycomb; UV; epidermis; stem cell; melanocyte; pigmentation; type II collagen

INTRODUCTION

The epidermis provides the body essential protection from external stressors. Solar UV irradiation, particularly its UVB component, is a key environmental stressor that can induce DNA damage in EpSCs which can lead to cancer (Dakup and Gaddameedhi, 2017; de Gruijl et al., 2001; Martens et al., 2018; Valejo Coelho et al., 2016). To combat the damaging effects of UV irradiation, EpSCs become pigmented in a process of transfer of melanin from melanocytes to EpSCs (Brenner and Hearing, 2008). Much of the knowledge about epidermal pigmentation came from studies of high doses of UV irradiation that cause DNA

damage in epidermal cells resulting in stabilization of p53 (Abdel-Malek et al., 2010; Chang et al., 2017; Cui et al., 2007; D'Orazio et al., 2006; Hachiya et al., 2001; Murase et al., 2009; Nguyen and Fisher, 2019). However, how EpSCs sense and respond to physiological low doses of UV that our body is exposed to on a daily basis and how this leads to epidermal pigmentation are not well understood.

Chromatin regulators are known to be sensitive to environmental agents (Aguilera et al., 2010; Alegria-Torres et al., 2011; Benayoun et al., 2015; Grönniger et al., 2010; Katiyar et al., 2012; Lämke and Bäurle, 2017). They can thereby serve as sensors through which UV irradiation mediates changes in gene expression leading to epidermal pigmentation. Polycomb repressive complex 1 (PRC1) and 2 (PRC2) are key chromatin repressors considered to be part of the paradigm for chromatin gene regulation (Simon and Kingston, 2009). Mammalian PRC2 complex contains the core subunits EED, SUZ12, and EZH1/2, which function together to establish trimethylation on histone H3 lysine 27 (H3K27me3) (Cao et al., 2002; Czermin et al., 2002; Dauber et al., 2016; Margueron and Reinberg, 2011; Simon and Kingston, 2009). The canonical mammalian PRC1 complex recognizes H3K27me3 and is recruited to chromatin (Bernstein et al., 2006; Lee et al., 2007; Wang et al., 2004). PRC1 contains an E3 ubiquitin ligase subunit, RING1A or RING1B, which catalyzes monoubiquitination on histone H2A lysine 119 (H2AK119ub) (de Napoles et al., 2004; Wang et al., 2004), a histone mark critical for Polycomb-mediated gene repression (Blackledge et al., 2020; Cohen et al., 2020; Cohen et al., 2018; Endoh et al., 2012). Together, PRC1 and PRC2 facilitate chromatin compaction and gene repression (Cao et al., 2002; Cohen et al., 2020; Cohen et al., 2021; Cohen et al., 2018; Schuettengruber et al., 2017). Polycomb-mediated gene repression is a tightly regulated process, and mutations in Polycomb group proteins have been shown to contribute to human diseases, including cancer (Perdigoto et al., 2012; Wang et al., 2015).

Here, we show that the levels of Polycomb proteins and Polycomb-dependent histone marks decrease in human and mouse epidermis exposed to a low dose of UV that does not induce extreme DNA damage or p53-stabilization. We show that ablation of key Polycomb subunits in adult mouse EpSCs, mimicking Polycomb depletion upon UV exposure, leads to a drastic increase in the number of melanocytes in the interfollicular epidermis (IFE) that are normally present only in hair follicles, causing epidermal pigmentation. By performing high-throughput transcriptional and chromatin analyses combined with *in vitro* and *in vivo* functional studies, we identified a critical regulator of melanogenesis and epidermal pigmentation: the extracellular matrix (ECM) protein COL2A1. We showed that *Col2a1* is a Polycomb target gene that is upregulated in UV-exposed EpSCs and that is sufficient to drive pigmentation production in melanocytes leading to epidermal pigmentation. Taken together, our study elucidates a Polycomb-*Col2a1* transcriptional axis that is induced in EpSCs by physiological exposure to UV to activate melanocytes and pigment the epidermis.

RESULTS

Loss of Polycomb repression in the epidermis results in epidermal pigmentation.

By performing immunohistochemical staining on UV-exposed (forearm) or UV-protected (buttocks) human skin, we found that EZH2, a key PRC2 subunit, and its corresponding

histone mark, H3K27me3, were significantly reduced in UV-exposed human epidermis compared to UV-protected human epidermis (Figure 1A–D). To test if Polycomb function is directly affected by physiological low doses of UV, we exposed mouse dorsal skin to a low dose of UVB, 1KJ/m^2, because it does not cause DNA damage analyzed by γ-H2AX foci or p53 stabilization compared to a high UVB dose (4KJ/m^2) (Figures 1E–F and S1A). We observed a dramatic reduction in the levels of EZH2 and H3K27me3 in murine epidermis one day after low dose UVB exposure (Figure 1G–J). The levels of RING1B, a key PRC1 subunit, and the H2AK119ub histone mark established by PRC1 were also reduced in UVB-exposed murine epidermis compared to the control (Figure 1K–N). Next, to dissect the mechanism of UV-induced reduction of Polycomb proteins in the epidermis, we exposed EpSCs to UVB *in vitro.* RT-qPCR analysis of RNA extracted from UVB-protected and UVB-exposed EpSCs showed that mRNA levels of both *Ezh2* and *Ring1b* were significantly reduced upon UVB exposure (Figure S1B). Western blot analysis revealed that EZH2 and RING1B protein levels also decreased upon UVB exposure, and they were slightly increased upon MG-132 treatment that blocks proteasomal degradation (Figure S1C). Together, these results led us to conclude that transcription and protein stability of key Polycomb subunits are reduced in the epidermis upon low dose UVB exposure.

To mimic the Polycomb depletion observed upon UV exposure, we generated an inducible, skin-specific PRC2-ablation (*Eed* iKO) mouse model. To do this, we crossed $Eed^{flox/flox}$ mice with *K14-CreERT2* mice (Li et al., 2000; Zhang et al., 2010), in which the ablation of a key PRC2 core subunit, EED, was induced in EpSCs and hair follicles following topical application of 4-hydroxyl-tamoxifen (4OH-Tam) onto the dorsal skin (Figure 2A). In *Eed* iKO mice, *K14-CreERT2* activation in postnatal (P) day 50 mice resulted in an efficient loss of H3K27me3 in the epidermis and hair follicle regions (Figure 2C). Immunofluorescence analysis showed no changes in cell death (Figure S1D), induction of DNA damage (Figure S1E), or immune cell infiltration (Figure S1F–G) but showed an increase in the proliferation of *Eed*-null EpSCs (Figure S1H). Interestingly, we observed drastic pigmentation of the *Eed* iKO skin, which was absent in the control dorsal skin (Figure 2B). Fontana-Masson staining showed that melanin is present in the epidermis of *Eed* iKO but not in the epidermis of control mice (Figure 2D–E). The observed pigmentation and loss of H3K27me3 in the *Eed* iKO mice persisted for at least 3 months after 4OH-Tam application and was not influenced by treatments applied at different stages of the hair cycle (Figure S2). Transmission electron microscopy (TEM) analysis showed the presence of isolated and well-organized melanosomes in both keratinocytes and melanocytes of *Eed* iKO mice but not in keratinocytes of control mice (Figure 2F). Taken together, these findings show that loss of *Eed* results in epidermal pigmentation.

To determine whether the observed pigmentation phenotype is caused by the loss of canonical repressive Polycomb function, we generated conditional inducible PRC1-null mice by crossing *K14-CreERT2* mice with *Ring1a*-null *Ring1b-floxed* mice (*K14-CreERT2;* $Ring1a^{-/-}$*;* $Ring1b^{flox/flox}$ *= Ring1a/b* i2KO) (Figure 2A). Topical application of 4OH-Tam in these mice resulted in the deletion of *Ring1b*, an essential PRC1 component, which led to the loss of H2AK119ub (Figure 2G). Because recent studies have shown that catalytic ubiquitylation activity of RING1B is required for Polycomb-mediated gene repression (Blackledge et al., 2020; Cohen et al., 2020; Cohen et al., 2018; Endoh et al., 2012;

Illingworth et al., 2015), we also generated conditional PRC1 catalytic-inactive mice (*K14-CreERT2; Ring1a*$^{-/-}$ *Ring1b*$^{I53A/flox}$ = *Ring1a/b* iI53A) in which the *Ring1b* gene carries an I53A point mutation that abrogates its E3-ligase activity, resulting in the loss of H2AK119ub (Figure 2G). Following 4OH-Tam application, we observed epidermal pigmentation and melanin accumulation in *Ring1a/b* i2KO and *Ring1a/b* iI53A epidermis, as observed in *Eed* iKO mice (Figure 2B and 2H–I). Together, these results show that loss of canonical Polycomb repression in the EpSCs leads to epidermal pigmentation.

Loss of Polycomb repression in the epidermis alters melanocyte behavior and localization.

In murine telogen skin, melanocyte stem cells (McSCs) are located in the bulge area of hair follicles, where they remain quiescent (Qiu et al., 2019). Immunofluorescence analysis of McSC/melanocyte markers dopachrome tautomerase (DCT) and receptor tyrosine kinase KIT (c-KIT) showed that McSCs were present in the hair follicles of all three Polycomb mutant skins (Figure S3A–B); however, compared to control skins, these cells became activated and proliferative (Figure S3A–B). We next asked whether loss of Polycomb leads to the presence of terminally differentiated pigment-producing melanocytes in the IFE because these cells are normally absent in the epidermis of murine dorsal skin (Figure 3A). Immunofluorescence analysis of DCT and c-KIT showed that melanocytes are present in the *Eed* iKO, *Ring1a/b* i2KO, and *Ring1a/b* iI53A IFE and confirmed their absence in control IFE (Figures 3B–C and S3C–E). The observed melanocytes were positive for tyrosinase-related protein 1 (TYRP-1), a marker of mature and fully differentiated melanocytes (Figure 3D–F) and were not proliferative (Figure S3F). We also generated mosaic *Eed*-null clones by treating mouse dorsal skins with a single dose of 4OH-Tam and observed that wild-type epidermal clones remained nonpigmented, whereas *Eed*-null IFE clones were pigmented and contained DCT-positive melanocytes (Figure 3G). Notably, levels of H3K27me3 did not change in melanocytes (Figure 3G), confirming that the *K14-CreERT2* ablation strategy does not target melanocytes and loss of Polycomb repression was restricted to epidermal cells. Overall, these observations show that loss of Polycomb repression in the epidermis leads to activation of McSCs and translocation of melanocytes to the IFE, resulting in epidermal pigmentation.

Given that reduction in Polycomb expression upon low UVB exposure occurs without inducing p53 stabilization and DNA damage, we wanted to ascertain whether the epidermal pigmentation phenotype observed in the Polycomb mutant epidermis was mediated through a p53-independent pathway. Thus, we performed phospho-p53 staining in both Polycomb mutant and control epidermis, which revealed no significant differences in phospho-p53 expression between them (Figure 3H). To further confirm that Polycomb-mutant-mediated pigmentation is p53-independent, we generated conditional inducible *Eed* and *p53* double knockout mice by crossing *K14-CreERT2* mice with *Eed-floxed* and *p53-floxed* mice (*K14-CreERT2; Eed*$^{flox/flox}$*; p53*$^{flox/flox}$ = *Eed/p53* i2KO) (Figure 3I). Topical application of 4OH-Tam in these mice resulted in the deletion of *Eed and p53,* leading to efficient loss of H3K27me3 and p53 (Figure 3J–K). Consistent with the observation that melanocytes are present in the epidermis and promote epidermal pigmentation in the Polycomb mutant mice, we also observed epidermal pigmentation and the presence of TYRP-1-positive melanocytes

in the *Eed/p53* i2KO epidermis (Figure 3L). Altogether, these results reveal that epidermal pigmentation observed in Polycomb mutant mice occurs via a p53-independent pathway.

Hair follicle stem cells (HFSCs) are known modulators of McSC activation (Chang et al., 2013; Lu et al., 2020; Tanimura et al., 2011). Because *K14-CreERT2*-mediated gene ablation targets both the IFE and HFSCs, we asked whether the epidermal pigmentation observed in Polycomb mutants is due to the loss of Polycomb in the EpSCs or in the HFSCs. We therefore generated *K15-CrePGR: Eed*$^{fl/fl}$ (*K15-Eed* iKO) mice in which topical application of RU-486, a progesterone agonist, resulted in efficient ablation of PRC2-dependent H3K27me3 specifically in the HFSCs and not in the epidermis (Figure 4A–C) (Morris et al., 2004). Remarkably, loss of *Eed* in HFSCs did not result in IFE pigmentation (Figure 4D). We also did not observe melanocytes in the epidermis of *K15-Eed* iKO mice, and the hair-follicle-associated McSCs remained non-proliferative (Figures 4E–F and S4A). Alternatively, to determine whether loss of Polycomb function in the IFE alone can cause epidermal pigmentation, we topically applied EZH2-specific inhibitors EPZ6438 and UNC1999 on the back skin of wild type mice (Knutson et al., 2013; Konze et al., 2013).This treatment caused selective loss of H3K27me3 in the epidermis and did not result in the loss of H3K27me3 in hair follicles (Figures 4G–H and S4B). In this epidermal-specific inhibition of EZH2, we observed an increased number of differentiated melanocytes in the IFE, leading to epidermal pigmentation (Figures 4H and S4C–D). To monitor changes in melanocyte behavior after the loss of Polycomb function in the EpSCs, we generated *TyrCreERT2;Rosa*$^{mT/mG}$ mice in which intraperitoneal injection of tamoxifen leads to GFP expression in McSCs. This allowed us to track the behavior of McSCs and melanocytes in the IFE treated with EZH2-specific inhibitors (Figure S4E). Interestingly, we observed that by day 14 of EZH2 inhibition, GFP+ melanocytes had begun to move away from the bulge to the IFE and that many GFP+ melanocytes had migrated into the IFE by day 18 (Figure S4F). These findings suggest that selective loss of Polycomb function in the EpSCs is sufficient to trigger melanocytes to migrate out of their homeostatic niche in the bulge region and translocate to the IFE.

Finally, by performing *in vitro* co-culturing of melanocytes with EpSCs, we observed an increase in pigment production in melanocytes co-cultured with *Eed*- or *Ring1a/b*-null EpSCs compared with melanocytes co-cultured with control EpSCs (Figure 4I). Taken together, these studies show that loss of canonical Polycomb repression in the epidermis, not in hair follicles, results in an increased number of melanocytes in the IFE, resulting in IFE pigmentation.

Loss of Polycomb repression in the epidermis induces the expression of UVB-signature genes.

To gain insight into the molecular mechanisms behind the observed IFE pigmentation phenotype, we conducted RNA-seq analysis of fluorescence-activated cell sorting (FACS)-purified EpSCs isolated from *Ring1a/b* i2KO, *Eed* iKO, and control mice (Figure S5). By performing differential gene expression analysis, we observed that the majority of differentially expressed genes were upregulated in Polycomb-null EpSCs compared with control EpSCs, with 117 genes upregulated in *Eed*-null EpSCs and 181 genes upregulated

in *Ring1a/b*-null EpSCs (Figure 5A and Table S1). We did not observe genes known to promote melanogenesis and epidermal pigmentation, such as stem cell factor (SCF; c-KIT ligand) or endothelin-3 (EDN3), among the genes upregulated in knockout cells (Table S1) (Garcia et al., 2008; Hachiya et al., 2001). A total of 47 genes were upregulated in both *Ring1a/b* i2KO and *Eed* iKO (Figure 5B). To determine the direct targets of PRC1/2 in EpSCs, we performed chromatin immunoprecipitation followed by high-throughput sequencing (ChIP-seq) assay for PRC1-dependent H2AK119ub and PRC2-dependent H3K27me3 histone marks (Bar et al., 2020). ChIP-seq analysis revealed that 66% of commonly upregulated genes were demarcated by both H2AK119ub and H3K27me3 in control EpSCs cells; therefore, these genes are direct targets of PRC1/2-mediated gene repression (Figure 5C and Table S2). Notably, among these genes, we identified ones known to be upregulated upon UVB irradiation, such as *Igfbp2, Hmga2, Col5a1, Sfrp2, Fbln2, Chst11, and Kcnk1* (Cho et al., 2018; Hachiya et al., 2009; Kim et al., 2016; Maier et al., 2016; McGrath et al., 2012; Moon et al., 2017; Qutob et al., 2018). Moreover, *Hmga2* is upregulated in UVB-irradiated epidermis and has been shown to promote McSCs translocation, and SFRP2 is upregulated in UVB-induced pigmented skin where it activates the WNT signaling pathway to promote melanogenesis (Kim et al., 2016; Moon et al., 2017). Using RT-qPCR, we confirmed our RNA-seq data showing that these UVB-induced genes are upregulated in PRC1/2-null EpSCs (Figure 5D). Together, our RNA-seq and ChIP-seq studies reveal that Polycomb functions in the EpSCs repress UVB-induced genes linked to the control of melanocyte behavior and function.

Type II collagen promotes epidermal pigmentation.

Gene ontology (GO) analysis of genes upregulated in both *Eed* iKO and *Ring1a/b* i2KO showed enrichment for pathways involved in protein secretion such as regulation of signaling and extracellular matrix organization (Figure 5E). We hypothesized that the de-repressed secretory proteins in Polycomb mutant EpSCs may function as paracrine factors to contribute to the epidermal pigmentation phenotype. To test this hypothesis, we selected the four candidates that were upregulated in PRC1-null and PRC2-null EpSCs: secreted frizzled-related protein 2 (SFRP2), insulin growth factor 2 (IGF2), type II collagen (COL2A1), and type V collagen 5 (COL5A1) (Figure 5F). We next established an *in vitro* system in which melanocytes were cultured in the presence of known melanogenesis-promoting proteins (SCF or EDN3) or each of the selected secretory proteins. As expected, when melanocytes were cultured in the presence of SCF or EDN3, we observed an increase in pigment production by melanocytes (Figure 6A–B). We did not observe changes in pigment production in melanocytes cultured with SFRP2, IGF2, or COL5A1. By contrast, melanocytes cultured with COL2A1 produced more melanin than negative controls (Figure 6A–B). ChIP-seq analysis of wild type EpSCs showed that *Col2a1* is demarcated by H3K27me3 and H2AK119ub histone marks, indicating that this gene is directly repressed by Polycomb complexes (Figure 6C). Western blot analysis also showed that loss of *Eed* or *Ring1a/b* in cultured EpSCs resulted in increased expression of COL2A1 compared with control EpSCs (Figure 6D–E). Furthermore, *in situ* hybridization and immunofluorescence analyses showed that both *Col2a1 mRNA* and COL2A1 protein were detected in *Eed* iKO and *Ring1a/b* i2KO epidermis but not in the control epidermis (Figure 6F–G). Notably, we observed that COL2A1 protein was not only present in the epidermis but also in the dermis

area near the upper hair follicle region (Figure S6A). Altogether, we concluded that loss of Polycomb leads to *Col2a1* expression in the EpSCs and that COL2A1 is secreted into the dermis region.

To test whether COL2A1 affects melanocyte behavior to promote epidermal pigmentation, we set up an EpSC and melanocyte co-culture system. By utilizing lentivirus infection, we generated EpSCs that ectopically express *Col2a1* (KC-Col2a1) and confirmed COL2A1 protein levels by Western blot (Figure S6B). Next, we co-cultured wild-type (KC) or KC-Col2a1 EpSCs with melanocytes (KC+MC and KC-Col2a1+MC, respectively) and observed a significant increase in melanin production in the KC-Col2a1+MC co-culture compared with control KC+MC or melanocyte-only (MC) cultures (Figures 7A–B and S6C). To test whether COL2A1 promotes expression of melanogenesis pathway-associated proteins, we cultured melanocytes directly on a COL2A1coated plate and non-coated or type I collagen (COL1A1)-coated plates, which served as negative controls. Western blot analysis showed that compared to melanocytes cultured on non-coated and COL1A1-coated plates, melanocytes cultured in the presence of COL2A1 showed increased expression of melanogenesis pathway-associated proteins such as TYRP-1 and tyrosinase (TYR) and activation of pMAPK signaling, which is known to regulate the production of melanin (D'Mello et al., 2016). Interestingly, the analysis of the AKT pathway that promotes melanocyte proliferation (Palmieri et al., 2015) showed no changes (Figure 7C). Next, we examined the effects of applying COL2A1 to wild-type skin *in vivo*. We performed intradermal injection of recombinant COL2A1 protein into the dorsal skin of wild-type mice and collected the injected area and surrounding dorsal skin 3 weeks post-injection. By performing Fontana-Masson staining, we observed that the COL2A1 injection resulted in a marked increase in skin pigmentation near the injected area, which was also accompanied by an increase in c-KIT(+) melanocytes (Figures 7D–E and S6D). These changes did not occur in the dorsal skin of mice injected with PBS (vehicle) or COL1A1, which served as negative controls (Figures 7D–E and S6D). Moreover, the migrated-melanocytes remained non-proliferative in the COL2A1-injected skin (Figure S6E). Thus, we conclude that COL2A1 induces changes in melanocyte behavior including migration, increased melanin production, and epidermal pigmentation, but it does not affect melanocyte proliferation.

UVB exposure leads to a loss of Ezh2 expression and decreased H3K27me3 levels in human and mouse epidermis (Figure 1). Because loss of Polycomb repression leads to COL2A1 expression in the dorsal skin of mice and results in the attraction of melanocytes and pigmentation, we asked whether UVB irradiation leads to epidermal COL2A1 expression. To test this, we exposed cultured EpSCs expressing scramble shRNA control (KC-sh-scr) or 2 different *Col2a1* shRNAs (KC-sh-Col2a1 −1 and −2) to UVB irradiation (20 mJ/cm^2) and tested for COL2A1 protein expression through Western blot analysis. We observed that COL2A1 expression significantly increased upon UVB exposure in KC-sh-scr and was reduced in KC-sh-Col2a1 cells, concluding that UVB induces the expression of COL2A1 protein (Figure 7F). To test whether UVB-exposed keratinocytes can induce changes in melanocyte behavior and promote pigmentation in a COL2A1-dependent manner, we exposed KC-sh-scr or KC-shCol2a1 EpSCs to UVB irradiation and then co-cultured them with melanocytes (KCsh-scr+MC and KC-sh-Col2a1+MC). We observed a significant increase in melanin production in the UVB-exposed KC-sh-scr+MC co-culture condition

and reduced pigmentation in the sh-Col2a1 co-culture condition (Figure 7G). Furthermore, by performing immunohistochemistry staining, we found that COL2A1 is increased in the epidermis of human UV-exposed skin compared with UV-protected skin (Figure 7H). Taken together, our study shows that UVB exposure leads to decreased Polycomb repression in the epidermis and therefore activation of UV-dependent gene expression, including expression of *Col2a1*. Epidermal COL2A1 leads to changes in melanocyte localization and increased melanogenesis, resulting in epidermal pigmentation.

DISCUSSION

Epidermal pigmentation, a mechanism by which melanocytes transfer melanin to epidermal cells, is critical in protecting EpSCs from DNA damage induced by UV irradiation (Brenner and Hearing, 2008). In this study, we uncover that the Polycomb-*Col2a1* axis in EpSCs controls epidermal pigmentation upon physiological UVB exposure. We showed that the expression of key Polycomb subunits, EZH2 and RING1B, and the levels of Polycomb-mediated repressive histone marks decrease in human and mouse epidermis upon UVB exposure. *In vivo* genetic studies mimicking Polycomb decrease in the epidermis upon UV exposure showed that ablation of Polycomb repression in murine EpSCs was sufficient to induce activation of McSCs and translocation of melanocytes to the IFE, causing epidermal pigmentation. High-throughput transcriptional and chromatin profiling revealed that many UVB-induced genes are under direct Polycomb control in adult EpSCs and are upregulated in Polycomb mutant EpSCs. Among these genes, we identified an ECM protein, COL2A1, as a critical regulator of melanocyte melanogenesis. Finally, we showed that COL2A1 is upregulated in UV-exposed human epidermis. Together, our data reveal how UVB irradiation directly alters Polycomb function in the epidermis to express *Col2a1* and pigment the epidermis.

Much of the knowledge about epidermal pigmentation came from studies where the epidermis was exposed to high doses of UV irradiation equivalent to sunburn. These studies have shown that high doses of UV cause DNA damage in EpSCs, leading to p53 stabilization and p53-mediated transcription of paracrine factors, α-melanocyte-stimulating hormone (α-MSH), adrenocorticotropic hormone (ACTH), and endothelin-1, which stimulates melanocytes (Abdel-Malek et al., 2010; Cui et al., 2007; Murase et al., 2009). Here, we show that a low dose of UVB irradiation, which does not cause severe DNA damage or p53 stabilization, leads to a decrease in the level of key Polycomb components, EZH2 and RING1B, and Polycomb-repressive histone marks. The loss of Polycomb in the epidermis, mimicking Polycomb decrease upon UV exposure, was sufficient to trigger melanocyte translocation to the IFE and epidermal pigmentation. Importantly, we did not observe p53 stabilization in Polycomb mutant epidermis (Figure S1D) and the *Pomc* (precursor of α-MSH and ACTH), and *Edn1* genes were not upregulated in *Eed* iKO or *Ring1a/b* i2KO EpSCs (Table S1). Moreover, we observed melanocytes are present in the *Eed/p53* i2KO IFE, leading to epidermal pigmentation (Figure 3L). Therefore, our findings provide evidence that melanocyte recruitment, increased melanogenesis, and epidermal pigmentation can be induced by a p53-independent mechanism and identify a role for Polycomb in these processes.

In human skin, melanocytes reside in the epidermis and hair follicles. In response to UV irradiation, melanocytes located in the epidermis interact with keratinocytes via physical contact or secreted factors, which leads to the synthesis and transfer of melanin to the neighboring keratinocytes. In adult murine skin, however, melanocytes are only located in the hair follicle bulge region, which serves as a niche to control McSC proliferation and differentiation to pigment the growing hair shaft (Qiu et al., 2019). Upon UVB irradiation, melanocytes get mobilized and move to the epidermis where they produce and transfer pigment to protect EpSCs from UV's harmful effects (Moon et al., 2017). Our studies show that the Polycomb-mediated pathway regulates each of these steps because loss of Polycomb in the epidermis leads to activation of McSCs, the presence of melanocytes in the IFE, and epidermal pigmentation without UV exposure. Analysis of RNA-seq data revealed that loss of Polycomb in the EpSCs resulted in the expression of *Col2a1*, an ECM protein that we showed in this study to be critical for melanogenesis; *Igf2, a* protein known to activate melanocyte proliferation (Edmondson et al., 1999; Mull et al., 2015); *Hmga2*, a regulator of McSC localization to the IFE upon UVB irradiation (Moon et al., 2017); and SFRP2, a secreted protein that promotes melanogenesis (Kim et al., 2016). Overall, the Polycomb complex has emerged as a critical transcriptional regulator of the epidermal pigmentation process. Moreover, we observed activation of genes known to control cell proliferation and motility with known roles in human diseases such as melanoma, including *Igfbp2*, a regulator of melanoma cell survival via the activation of insulin growth factor (IGF) signaling pathway (Strub et al., 2018); *Fbln2*, a secreted extracellular matrix glycoprotein that is expressed in several tumor types and controls cell motility (Timpl et al., 2003); *Chst11*, a chondroitin 4-O sulfotransferase involved in promoting metastasis in breast cancer (Cooney et al., 2011); and *Col5a1*, a collagen that regulates cell proliferation and invasion in ovarian cancer (Zhang et al., 2021). Future studies will uncover the roles of the Polycomb-mediated pathway in controlling melanocyte behavior and melanoma formation.

Our studies identified COL2A1 as an important regulator of melanogenesis. Whereas COL2A1 is normally absent in the skin, it is upregulated in the epidermis upon UV exposure, demonstrating the unique role of this protein in the UV-induced epidermal response. Growing evidence indicates the importance of ECM proteins in response to UV irradiation. In fibroblasts, UV irradiation has been shown to stimulate the expression of the ECM protein CCN1, resulting in increased melanogenesis through activation of MAPK-kinase signaling pathways in melanocytes (Xu et al., 2018). Another example is the ECM protein laminin332, which interacts with the integrin α6β1 receptor present on melanocytes to promote melanogenesis (Chung et al., 2014; Chung et al., 2011). Our studies showed that COL2A1 promotes the melanogenesis via activation of MAPK pathway in melanocytes to regulate the production of melanin (Figure 7C). However, further work is needed to determine how COL2A1 interacts with melanocytes to regulate pigment production.

The canonical model of Polycomb-mediated gene control postulates that PRC1 and PRC2 facilitate each other's recruitment to chromatin to exert transcriptional repression (Schuettengruber et al., 2017; Simon and Kingston, 2013). Although the role of PRC1 and PRC2 in the regulation of epidermal development has been well studied (Bar et al., 2019; Cohen et al., 2018; Cohen et al., 2019; Dauber et al., 2016), the roles of the Polycomb complex in the control of adult EpSCs during homeostasis or upon stress are

unknown and are studied here. We show that loss of either PRC1 or PRC2 or expression of a catalytically inactive form of RING1B (I53A) in the adult murine EpSCs results in an identical phenotype of epidermal pigmentation. Upon UV irradiation, the level of key Polycomb subunits, EZH2 and RING1B, and Polycomb-repressive histone marks decrease in the epidermis, allowing for de-repression and activation of genes needed to avert the effects of UV damage.

Our studies propose future avenues for investigating how uncovered molecular mechanisms contribute to UVB-mediated skin disorders such as cancer. Polycomb proteins are often mutated in skin squamous cell carcinoma (SCC) (Wang et al., 2015), and it will be interesting to identify how these mutations cooperate with UVB-mediated processes to promote SCC tumorigenesis. It will also be worth investigating how the uncovered processes affect melanoma, one of the deadliest and aggressive skin cancers (Schadendorf et al., 2018). Indeed, we show that changes in EpSCs affect the localization and function of wild-type melanocytes. It will thus be interesting to identify whether changes in the epidermis cooperate with mutations in melanocytes to lead to melanoma. Furthermore, narrow-band UVB phototherapy is a prevalent treatment for vitiligo (Goldstein et al., 2015), a depigmenting disorder that selectively destroys melanocytes. Although phototherapy has been shown to be generally effective for treating vitiligo, it is not devoid of the harmful effects of UVB. Hence, a UVB-independent melanogenesis-inducing treatment would be highly beneficial for individuals with this disease. Here we have identified a Polycomb-mediated process that is sufficient in increasing melanogenesis without inducing DNA damage or an inflammatory response, which are side effects of UVB. Interestingly, epidermal application of the EZH2-specific inhibitors, EPZ6438 and UNC1999, also resulted in an epidermal pigmentation phenotype similar to that of Polycomb-null epidermis. Therefore, developing products modeled after the EZH2-specific inhibitors used in this study will be an attractive alternative to phototherapy for vitiligo patients.

Limitations of the study

We found that low-dose UV exposure leads to both transcriptional and translational downregulation of key Polycomb proteins in the EpSCs. However, the mechanism by which UV exposure leads to changes in Polycomb levels remains unclear and they will be studied in the future.

STAR METHODS

RESOURCE AVAILABILITY

Lead contact—Further information and requests for resources and reagents should be directed to and will be fulfilled by the lead contact Elena Ezhkova, (elena.ezhkova@mssm.edu)

Materials availability

Mouse EpSCs cell lines generated in this study are available from the lead contact’s laboratory.

Data and code availability

The accession number for the sequencing data reported in this manuscript is GSE159767.

This paper does not report original code.

METHOD DETAILS

Mice

All the mice used in this study were housed at the Center of Comparative Medicine and Surgery (CCMS) at Icahn School of Medicine at Mount Sinai (ISMMS) according to the Institutional Animal Care and Use Committee (IACUC) guidelines (Protocol number LA11–0020). *K14-CreERT2* mice were kindly provided by Dr. Tudorita Tumbar (Zhang et al., 2010). *K15-CrePGR1* mice (Stock number: 005249), $p53^{LoxP}$ mice (Stock number: 008462), *Tyr-CreERT2* (Stock number: 012328), and $Rosa^{mTmG}$ (Stock number: 007676) were obtained from Jackson Laboratories. $Eed^{flox/flox}$ mice were kindly provided by Drs. Weipeng Mu and Terry Magnuson (Mu et al., 2014). $Ring1a^{-/-}$and $Ring1b^{flox/flox}$ mice, kindly provided by Dr. Miguel Vidal, were previously described (Calés et al., 2008; del Mar Lorente et al., 2000). $Ring1b^{I53A}$ mice were kindly provided by Dr. Wendy A. Bickmore (Illingworth et al., 2015). Mice were genotyped by PCR using tail DNA that was extracted using DirectPCR Lysis Reagent (Viagen Biotech Inc.) according to the manufacturer's instructions. Both male and female mice were used in this study. Primer sequences used for genotyping are listed in Supplemental Table S3.

Human skin samples

Paraffin-embedded (FFPE) human skin tissue sections were obtained from the University of Pennsylvania Skin Biology and Disease Resource Center (SBDRC). UVB-protected and -exposed samples from the buttocks and forearms of the same patient or a similar patient matched for age and gender were used for IHC studies.

Cell cultures

Primary epidermal stem cells (EpSCs) were isolated from newborn mouse epidermis as previously described (Cohen et al., 2018). Primary EpSCs were derived from P0 newborn *K14-CreERT2;* $Eed^{flox/flox}$, *K14-CreERT;* $Ring1a^{-/-}$*;* $Ring1b^{flox/flox}$, and control mice and were cultured in E media (Nowak and Fuchs, 2009), supplemented with 15% fetal bovine serum (FBS, R&D Systems) and 0.3mM $CaCl_2$ and plated on a feeder layer of mitomycin C-treated 3T3 fibroblasts. EpSCs were dissociated with 0.25% Trypsin/EDTA (Corning) and grown in E media with 15% FBS and 0.05mM $CaCl_2$. Keratinocytes were cultured in 7.5% CO_2 at 37°C. To conditionally delete *Ring1b* in *K14-CreERT;* $Ring1a^{-/-}$*;* $Ring1b^{flox/flox}$ or to delete *Eed* in *K14-CreERT2;* $Eed^{flox/flox}$ in culture experiments, cells were treated with 1mM hydroxyl-tamoxifen (Sigma-Aldrich) once daily for 6 days. HEK293T (used for lentivirus production) and B16F0 (for keratinocyte-melanocyte co-cultures) cells were cultured in DMEM with 10% FBS and 1% pen/strep solution (Corning) in 5% CO_2 at 37°C. For co-cultures, melanocytes (B16F0) and EpSCs were plated in 1:5 ratio in E media with 15% FBS supplemented with 0.05mM $CaCl_2$ in 7.5% CO_2 at 37°C.

Drug treatments

For hydroxyl-tamoxifen (4OH-Tam, Sigma-Aldrich) topical treatment to induce the Polycomb ablation using *K14-CreERT2*, 4OH-Tam was dissolved in absolute ethanol (Sigma-Aldrich) to a final concentration of 10mg/ml. To induce recombination, 100μl (1mg) of 4OH-Tam was topically applied on shaved dorsal skin of postnatal day 50 (P50) mice once per day for 4 days. Control mice were treated with the same amount of absolute ethanol. For mosaic induction of *Eed* iKO, 100μl of 4OH-Tam was topically applied once to shaved dorsal skin of P50 mice. To induce *Eed* ablation only in the hair follicle bulge using *K15-CrePGR*, RU-486 (Cayman Chemicals) was dissolved in 100% ethanol (Sigma-Aldrich) to a final concentration of 10 mg/ml. 100μl of RU-486 was topically applied on shaved dorsal skin of P50 mice once per day for 7 days. For fate mapping of bulge-associated McSCs, P50 *Tyr-CreERT2; Rosa*$^{mT/mG}$ mice were injected intraperitoneally with tamoxifen (Sigma-Aldrich) at doses of 100μg per gram of body weight for 3 consecutive days. For intradermal collagen injection, type I and type II collagen (Sigma-Aldrich) were dissolved in sterile 0.2% acetic acid in 1XPBS to a final concentration of 1mg/ml. In addition, 100μg of type I or type II collagen were injected intradermally into the dorsal skin of P50 mice. Control mice were injected with an equivalent volume of 1X PBS. The injection sites were marked using water-resistant ink. For the topical treatment of EZH2 inhibitors, a 1cm^2 area of the dorsal skin of P50 mice was shaved, and 20μl of 5mM UNC1999, 10mM EPZ6438, or DMSO (Sigma-Aldrich) were applied to the shaved skin area. Topical applications were performed once daily from P50 to P70. For MG-132 treatment, EpSCs were incubated with 4μm MG-132 (Selleckchem) or DMSO (control) for 4 hours.

Lentivirus generation and infection

For ectopic type II collagen (*Col2a1*) expression, HEK293T cells were transfected with 10μg of pLX304-Col2a1 lentiviral construct (Horizon Discovery lentiviral library), 10μg packing plasmids (psPAX2, pMD2.G, and Addgene plasmids 12259 and 12260—a generous gift from Didier Trono), and 20μl jetPEI transfection regent (Polyplus) according to the manufacturer's instructions. For *Col2a1* shRNA knockdown, HEK293T cells were transfected with the 10μg pLKO-Col2a1 shRNA (sequences listed in Table S3) lentiviral construct (Sigma-Aldrich), 10μg packing plasmids (psPAX2, pMD2.G), and 20μl jetPEI transfection regent. Lentivirus-containing media were collected 48 hours post transfection and filtered through a 0.45mm filter. EpSCs were then transduced with viral stock and supplemented with 4μg/ml polybrene (Sigma-Aldrich). Virus-containing media were replaced 8 hours post infection with fresh E media with 15% FBS and 0.05mM $CaCl_2$, and cells were cultured for an additional 48 hours. For ectopic *Col2a1* expression, infected cells were selected with 0.4μg/mL Blasticidin S (Sigma-Aldrich). For *Col2a1* shRNA, cells were selected with 5μg/mL puromycin (Sigma-Aldrich) for 3 days.

Melanin content analysis

For Polycomb mutant co-culture experiments, Polycomb mutant EpSCs (*Eed* iKO or *Ring1a/b* i2KO) were co-cultured with B16F0 melanocytes in E media supplemented with 15% FBS and 0.05mM $CaCl_2$ in 7.5% CO_2 at 37°C for 72 hours. For melanogenesis assays

of candidate melanogenesis-promoting proteins, 50,000 B16F0 cells were plated in 6-well plates and were treated with 100μg/ml endothelin-3 (EDN-3) (R&D systems); 100μg/ml stem cell factor (SCF) (R&D systems); 100μg/ml secreted frizzle-related protein 2 (SFRP2) (R&D systems); 50μg/ml insulin-like growth factor 2 (IGF2) (R&D systems); and 10μg/ml type I, II, and V collagen (COL1A1, COL2A1, and COL5A1) (Sigma-Aldrich) for 48 hours. For UVB irradiation, UVB-irradiated keratinocytes were co-cultured with B16F0 cells in E media supplemented with 15% FBS and 0.05mM $CaCl_2$ in 7.5% CO_2 at 37°C for 5 days. For melanin content analysis, all culture conditions were washed with PBS, harvested in 1N NaOH containing 10% DMSO, and then heated at 80°C for 90 minutes for melanin extraction. The absorbance of extracted melanin was measured at 450nm using an ELISA microplate reader (SpectraMax M5, Molecular Devices).

Transmission electron microscopy

Transmission electron microscopy (TEM) was performed in the Core Pathology Electron Microscopy Facility, Icahn School of Medicine at Mount Sinai. Dorsal skin was collected from P71 *Eed* iKO, and control mice were then immediately fixed in 3% glutaraldehyde with 0.2M sodium cacodylate at pH 7.4. After overnight fixation, the fixative solution was removed and replaced with a phosphate buffer followed by 1% osmium tetroxide buffered with sodium cacodylate. After one hour, osmium tetroxide was replaced with increasing concentrations of ethanol through propylene oxide and into Embed 812. The plastic sections were cut in 1μm, stained with methyl blue and azure II, and observed by light microscopy. The ultrathin sections were cut on a Leica Ultracut UCT ultramicrotome and observed with a Hitachi H-7650 transmission electron microscope (Hitachi High–Technologies Instrumentation, Tokyo, Japan) linked to an SIA (Scientific Instruments and Applications) digital camera controlled by Maxim CCD software.

Fluorescence-activated cell sorting

FACS isolation of EpSCs from control, *Eed* iKO, and *Ring1a/b* i2KO were performed as follows: Adult dorsal skin was collected from control, *Eed* iKO, and *Ring1a/b* i2KO mice; washed with 1× PBS; and incubated in 0.25% Trypsin/EDTA (Corning) at 37°C for one hour. After incubation, cell suspensions were strained through 40μm filters (Thermo Fisher Scientific) and washed twice with 1× DPBS (Corning). The cells were stained with 1:200 PerCP-Cy5.5-Sca1 (Thermo Fisher Scientific), 1:200 FITC-α6-integrin (Thermo Fisher Scientific), and 1:100 APC-EpCAM (Biolegend) for 30 minutes on ice and then washed twice with 1× DPBS before cell sorting. Interfollicular epidermis, enriched for EpSCs, was sorted as EpCAM(+), Sca1(+), and α6-integrin (high). For ChIP and ChIP-Seq analyses, cell suspensions were stained for cell viability using Zombie violet (Biolegend), and cells were cross-linked with 1% formaldehyde for 10 minutes at room temperature. Cross-linking was stopped by adding 125mM glycine for 5 minutes at room temperature, followed by 2 washes with 1× DPBS, before staining and FACS sorting as described above. All cell isolations were performed on a FACS IMI5L instrument (BD) in the Flow Cytometry Core Facility at Icahn School of Medicine at Mount Sinai.

RNA purification, RT-qPCR, and RNA-seq library preparation

A total of 5×10^4 FACS-purified cells were collected directly into RLT Plus buffer (QIAGEN), and total RNA was isolated with the RNeasy Plus Micro Kit (QIAGEN) and DNase1 treatment (QIAGEN) according to the manufacturer's instructions. cDNA was reverse-transcribed from total RNA using qScript cDNA SuperMix (Quanta Biosciences) according to the manufacturer's instructions. Samples were analyzed by RT-qPCR using LightCycler® 480 SYBR Green I Master Mix (Roche) on a LightCycler 480 instrument (Roche). Results were normalized to *GAPDH* mRNA levels. Primer sequences are available in Supplemental Table S3. For RNA-seq library preparation, the total RNA quality was measured using a Bioanalyzer (Agilent), and samples with RNA integrity numbers (RIN) > 8 were used. Then 10ng of total RNA were reverse-transcribed and amplified using the Ovation RNA-seq System V2 (NuGEN). Libraries were constructed from 100ng of sonicated cDNA (Covaris M220) using the Ovation Ultralow system V2 (NuGEN). The concentration and quality of the libraries were determined using Qubit (Invitrogen) and Bioanalyzer (Agilent). Constructed RNA-seq libraries were sequenced at GENEWIZ on the Illumina HiSeq platform, obtaining 150 nucleotide paired-end reads.

Chromatin immunoprecipitation (ChIP) and ChIP-seq library preparation

ChIP was performed on FACS-purified populations using materials and methods as previously described (Bar et al. 2020). We used 3×10^5 FACS-purified cells per ChIP to profile H3K27me3 and H2AK119ub histone marks. FACS-purified cells were incubated in lysis buffer 1 (50mM HEPES pH = 7.5, 140mM NaCl, 1mM EDTA, 10% glycerol, 0.5% NP-40, 0.25% Triton X-100, protease inhibitor cocktail [Roche]) for 10 minutes on ice, then incubated for 10 minutes with lysis buffer 2 (10mM Tris-HCl pH = 7.5, 200mM NaCl, 1mM EDTA, 0.5mM EGTA). Before ChIP, cells were resuspended in lysis buffer 3 (10mM Tris-HCl pH = 8.0, 100mM NaCl, 1mM EDTA, 0.5mM EGTA, 0.1% Na-deoxycholate, 0.5% N-laurolsarcosine, 1% Triton X-100) and sonicated using a Bioruptor Sonicator (Diagenode, UCD-200) according to a 25× regimen of 30 seconds of sonication followed by 90 seconds of rest at 4°C. The cell lysate was incubated overnight at 4ºC with antibodies as indicated in Supplemental Table S3. Dynal protein G magnetic beads (Invitrogen) were added the next day and incubated for 6 hours at 4ºC. The beads were sequentially washed with low salt (20mM Tris-HCl pH = 8.0, 150mM NaCl, 2mM EDTA, 0.1% SDS, 1% Tritonx X-100), high salt (20mM Tris-HCl pH = 8.0, 500mM NaCl, 2mM EDTA, 0.1% SDS, 1% Tritonx X-100), LiCl (20mM Tris-HCl pH = 8.0, 250mM LiCl, 1mM EDTA, 1% Na-deoxycholate, 1% NP-40), and Tris-EDTA (50mM Tris-HCl pH = 8.0, 1mM EDTA) buffers for 10 minutes each at 4ºC. Bound chromatin was eluted, and cross-linking was reversed by overnight incubation at 65ºC, followed by 0.15mg/ml RNase A (Sigma-Aldrich) and 0.3mg/ml proteinase K (Roche) treatments. Samples were purified using a ChIP DNA Clean and Concentrator kit (Zymo Research). For high-throughput ChIP sequencing, libraries were constructed from 5ng of purified DNA using the NEBnext Ultra II DNA Library Prep Kit (New England Biolabs) according to the manufacturer's instructions. Constructed ChIP-seq libraries were sequenced on Illumina NextSeq 500 platform with 75 single-end reads in the Oncological Sciences NextSeq Facility, Icahn School of Medicine at Mount Sinai, and two biological replicates were used.

Western blotting

Cells were collected and lysed by the addition of EZ lysis buffer (60mM Tris-HCl pH = 6.8, 10% glycerol, 2% SDS) for 10 minutes at 95 ºC. Samples were run on 10% SDS-PAGE, transferred to PVDF membranes, and analyzed with the indicated antibodies in Supplemental Table S3.

Immunofluorescence, *in situ* hybridization and microscopy

Dorsal skin tissues were collected from adult mice, embedded in OCT compound (Tissue-Tek), and subsequently cut into 8μm sections using a Leica Cryostat. Slides were then pre-fixed in 4% PFA for 10 minutes at room temperature and blocked for one hour at room temperature in blocking solution (1× PBS supplemented with 0.3% Triton X-100, 1% BSA, 0.25% normal donkey serum, 0.01% gelatin). Primary antibodies were diluted in blocking solution and incubated overnight at 4ºC. Slides were then incubated with secondary antibodies for one hour at room temperature. Slides were counterstained with DAPI to visualize nuclei. All antibodies and dilutions are available in Supplemental Table S3. *In situ* hybridization for Col2a1 was performed using RNAscope probes and a 2.5HD-RED detection kit (Advanced Cell Diagnostics) according to the manufacturer's protocol. Slides were imaged using a Leica DM5500 slide microscope. For each immunofluorescence assay, at least 3 animals from at least 2 independent litters were analyzed per mutant genotype.

Immunohistochemistry

Formalin-fixed, paraffin-embedded 5μm sections of UVB-protected and -exposed human skin were obtained from Penn SBDRC. Sections were deparaffinized in xylene and rehydrated in decreasing concentrations of ethanol. Tissues were then subjected to antigen retrieval with 10mM sodium citrate buffer pH = 6.0 and treated with 1% H_2O_2 in methanol for 10 minutes. The slides were incubated with 2.5% normal horse blocking serum at room temperate for 30 minutes and stained with 1:250 mouse anti-EZH2 antibodies (BD Biosciences), 1:500 rabbit anti-H3K27me3 antibodies (MilliporeSigma), 1:200 rabbit anti-COL2A1 (Abcam), or control 1:200 rabbit IgG antibodies (MilliporeSigma) overnight at 4ºC. The slides were then incubated with secondary anti-rabbit HRP for one hour at room temperature using the ImmPRESS Polymer Detection Kit according to the manufacturer's instructions (Vector Laboratories), and the staining was developed using the DAB peroxidase substrate kit (Vector Laboratories). To identify nuclei, slides were counterstained with hematoxylin. Fontana-Masson staining was performed using the Fontana-Masson Stain Kit (Sigma-Aldrich) according to the manufacturer's instructions.

UVB irradiation

For mouse dorsal skin, C57BL/6J mice were shaved, and topical depilatory cream (Nair©) was used prior to irradiation. Mice dorsal skin was exposed to UV irradiation in a custom-made Lucite chamber (Plastic Design Corporation) outfitted with a double bank of UVB lamps (Analytik Jena). UV emittance was measured with a UV photometer (UV Products) equipped with UVB measuring head. In addition, 1KJ/m^2 and 4KJ/m^2 was calculated as the UV dose of radiation exposed on the dorsal skin. The skin was collected 24 hours post-UV exposure. For *in vitro* experiments, EpSCs were irradiated with 20mJ/cm^2 once using a

UVB lamp (OSRAM), and the UV dose was calculated using a UV photometer (General Tools). UV-irradiated cells were collected 4 days after exposure for western blotting or co-culture experiments.

QUANTIFICATION AND STATISTICAL ANALYSIS

RNA-seq data analysis

The RNA-seq reads were aligned to the mouse transcriptomes corresponding to the GENCODE annotation (vM20) (Harrow et al., 2012) using the software Kallisto (v0.42.5) (Bray et al., 2016). The protein-coding genes with an average TPM (transcripts per million reads mapped) > 1 in control, *Eed* iKO or *Ring1a/b* i2KO, were used for differential gene expression analysis with the software DESeq2 (Love et al., 2014) at a significance level of adjusted p-value < 0.05 and more than 2-fold changes to compare the gene expression changes across different genotypes and their controls (*Eed* iKO vs Ctrl, *Ring1a/b* i2KO vs Ctrl).

ChIP-seq analysis and data visualization

Data processing, peak calling, and associating peaks to genes for the H3K27me3 and H2AK119ub ChIP-seq data were previously described (Cohen et al., 2018; Zhao and Zheng, 2018). Peaks called in both replicates were used. For visualization, we used the Integrative Genomics Viewer (IGV; http://software.broadinstitute.org/software/igv/) and TDF files from the igvtools (v2.3.57; https://software.broadinstitute.org/software/igv/igvtools).

Gene ontology enrichment analysis

Identification of significantly overrepresented functional categories was done using the DAVID tool on the default setting (Huang da et al., 2009). Selected GO terms were considered significant with $p < 0.05$. Genes significantly upregulated in *Eed* iKO vs. control and *Ring1a/b* i2KO vs. control epidermal cells were annotated using the same significance parameters and selected GO terms are shown in Figure 5E and Supplemental Table S1.

Quantification of EZH2, H3K27me3, and COL2A1 in human skin

EZH2(+) or H3K27me3(+) cells in the basal layer of the epidermis were quantified using ImageJ software. Hematoxylin staining was used to quantify the total number of nuclei in the basal layer, and the data are shown as the percentage of EZH2(+) or H3K27me3(+) nuclei in the basal layer of the epidermis. At least 10 random epidermal regions were measured for each group from 5 UV-protected and 7 UV-exposed skin samples. COL2A1 signal intensity in the epidermis was quantified using ImageJ software. Briefly, for UV-protected and UV-exposed skin epidermis, the channels of hematoxylin and DAB images were separated to analyze the specific emission channel. The mean intensity of DAB signals was calculated with ImageJ software. At least 5 random epidermal regions were measured for each group from 8 UV-protected and 8 UV-exposed skin samples.

Quantification of Polycomb function in UVB-protected or-exposed mice

EZH2(+), H3K27me3(+), RING1B(+), or H2AK119ub(+) cells in the basal layer of the epidermis were quantified using ImageJ software. DAPI staining was used to quantify the total number of nuclei in the basal layer, and the data are shown as the percentage of EZH2(+), H3K27me3(+), RING1B(+), or H2AK119ub(+) nuclei in the basal layer of the epidermis. At least 10 random epidermal regions were measured for each group from 3 UVB-protected and 3 UVB-exposed mice.

Quantification of DCT, TYRP-1, and c-KIT melanocyte

Melanocytes were quantified by the number of DCT, TYRP-1, or c-KIT(+) cells per millimeter (mm) of skin. Sections had typical skin length ranging between 7 and 14mm. At least 100mm of total skin length was analyzed per condition. At least 3 animals from at least 2 independent litters were used for each mutant genotype. Comparisons and statistics were analyzed between matching Polycomb mutants and control mice or EZH2 inhibitor-treated and DMSO-treated control skin.

Quantification of pigment epidermis area

Melanin of the Polycomb KO and control skins were detected by Fontana-Masson staining. Pigment areas were measured over the epidermal surface by using ImageJ software. The area of epidermal pigmentation is depicted as a percentage of measurement of pigmented area divided by total epidermal surface area. Skin pigmentation was analyzed per condition from at least 3 animals from at least 2 independent litters per mutant genotype. Comparisons and statistics were performed between matching Polycomb KO and control mice.

Statistics

To determine the statistical significance between 2 groups, a Student's *t*-test was performed. To determine the statistical significance among more than 2 groups, comparisons were made using one-way ANOVA with the Tukey post-hoc test correction for multiple comparisons. All data in bar graphs are presented as mean ± SD. The number of biological replicates used for comparison is indicated in each figure. For each comparison, at least 3 animals for each group from 2 independent litters were used. Significance levels were defined as *$p < 0.05$, **$p < 0.01$, ***$p < 0.001$, or NS (not significant). For statistical analyses, GraphPad Prism 8 was used. No randomization or blinding was performed in this study. Sample size is indicated in figure legends, and statistical methods are indicated in the quantification and statistical analysis paragraph.

Supplementary Material

Refer to Web version on PubMed Central for supplementary material.

ACKNOWLEDGMENTS

We thank Sergei Ezhkov and all Ezhkova lab members for their help and critical suggestions. We thank Dr. Miguel Vidal for the *Ring1a*-null and *Ring1b-floxed* mice, Drs. Weipeng Mu and Terry Magnuson for the *Eed-floxed* mice, and Dr. Tudorita Tumbar for the *K14-CreERT2* mice. We thank Dr. Emily Bernstein for B16F0 cells and Penn SBDRC for human skin samples. We also thank the Flow Cytometry Core, the Electron Microscopy Facility, and the Tisch Cancer Center sequencing facility at the ISMMS. Research reported here was supported by the

National Institutes of Health under award numbers R01AR069078 (to E.E.), R01HL148128 and R01HL153920 (to D. Zheng), R01GM122749 and P30CA196521 (to J.J.), an endowed professorship from the ISMMS (to J.J.), the Tisch Cancer Institute P30 Cancer Support Grant (to E.E.), and the NYSTEM Institutional Training program C32561GG (to P.F.).

DECLARATION OF INTEREST

The Jin laboratory received research funds from Celgene Corporation, Levo Therapeutics, and Cullgen, Inc. J.J. is a cofounder, equity shareholder and consultant of Cullgen, Inc.

REFERENCES

Abdel-Malek ZA, Kadekaro AL, and Swope VB (2010). Stepping up melanocytes to the challenge of UV exposure. Pigment Cell & Melanoma Research 23, 171–186. [PubMed: 20128873]

Aguilera O, Fernandez AF, Munoz A, and Fraga MF (2010). Epigenetics and environment: a complex relationship. J Appl Physiol (1985) 109, 243–251. [PubMed: 20378707]

Alegria-Torres JA, Baccarelli A, and Bollati V. (2011). Epigenetics and lifestyle. Epigenomics 3, 267–277. [PubMed: 22122337]

Bar C, Cohen I, Zhao D, Pothula V, Litskevitch A, Koseki H, Zheng D, and Ezhkova E. (2019). Polycomb Repressive Complex 1 Controls Maintenance of Fungiform Papillae by Repressing Sonic Hedgehog Expression. Cell Rep 28, 257–266 e255. [PubMed: 31269445]

Bar C, Valdes VJ, and Ezhkova E. (2020). Chromatin Immunoprecipitation of Low Number of FACS-Purified Epidermal Cells. Methods Mol Biol 2154, 197–215. [PubMed: 32314219]

Benayoun BA, Pollina EA, and Brunet A. (2015). Epigenetic regulation of ageing: linking environmental inputs to genomic stability. Nature Reviews Molecular Cell Biology 16, 593–610. [PubMed: 26373265]

Bernstein E, Duncan EM, Masui O, Gil J, Heard E, and Allis CD (2006). Mouse Polycomb Proteins Bind Differentially to Methylated Histone H3 and RNA and Are Enriched in Facultative Heterochromatin. Molecular and Cellular Biology 26, 2560–2569. [PubMed: 16537902]

Blackledge NP, Fursova NA, Kelley JR, Huseyin MK, Feldmann A, and Klose RJ (2020). PRC1 Catalytic Activity Is Central to Polycomb System Function. Mol Cell 77, 857–874 e859. [PubMed: 31883950]

Bray NL, Pimentel H, Melsted P, and Pachter L. (2016). Near-optimal probabilistic RNA-seq quantification. Nat Biotechnol 34, 525–527. [PubMed: 27043002]

Brenner M, and Hearing VJ (2008). The protective role of melanin against UV damage in human skin. Photochemistry and photobiology 84, 539–549. [PubMed: 18435612]

Calés C, Román-Trufero M, Pavón L, Serrano I, Melgar T, Endoh M, Pérez C, Koseki H, and Vidal M. (2008). Inactivation of the polycomb group protein Ring1B unveils an antiproliferative role in hematopoietic cell expansion and cooperation with tumorigenesis associated with Ink4a deletion. Mol Cell Biol 28, 10181028.

Cao R, Wang L, Wang H, Xia L, Erdjument-Bromage H, Tempst P, Jones RS, and Zhang Y. (2002). Role of histone H3 lysine 27 methylation in Polycomb-group silencing. Science 298, 1039–1043. [PubMed: 12351676]

Chang C-H, Kuo C-J, Ito T, Su Y-Y, Jiang S-T, Chiu M-H, Lin Y-H, Nist A, Mernberger M, Stiewe T, et al. (2017). CK1α ablation in keratinocytes induces p53-dependent, sunburn-protective skin hyperpigmentation. Proceedings of the National Academy of Sciences, 201702763.

Chang C-Y, Pasolli HA, Giannopoulou EG, Guasch G, Gronostajski RM, Elemento O, and Fuchs E. (2013). NFIB is a governor of epithelial–melanocyte stem cell behaviour in a shared niche. Nature 495, 98–102. [PubMed: 23389444]

Cho BA, Yoo SK, and Seo JS (2018). Signatures of photo-aging and intrinsic aging in skin were revealed by transcriptome network analysis. Aging (Albany NY) 10, 1609–1626. [PubMed: 30021930]

Chung H, Jung H, Lee JH, Oh HY, Kim OB, Han IO, and Oh ES (2014). Keratinocyte-derived laminin-332 protein promotes melanin synthesis via regulation of tyrosine uptake. J Biol Chem 289, 21751–21759. [PubMed: 24951591]

Chung H, Suh EK, Han IO, and Oh ES (2011). Keratinocyte-derived laminin-332 promotes adhesion and migration in melanocytes and melanoma. J Biol Chem 286, 13438–13447. [PubMed: 21349841]

Cohen I, Bar C, and Ezhkova E. (2020). Activity of PRC1 and Histone H2AK119 Monoubiquitination: Revising Popular Misconceptions. Bioessays 42, e1900192.

Cohen I, Bar C, Liu H, Valdes VJ, Zhao D, Galbo PM Jr., Silva JM, Koseki H, Zheng D, and Ezhkova E. (2021). Polycomb complexes redundantly maintain epidermal stem cell identity during development. Genes Dev 35, 354–366. [PubMed: 33602871]

Cohen I, Zhao D, Bar C, Valdes VJ, Dauber-Decker KL, Nguyen MB, Nakayama M, Rendl M, Bickmore WA, Koseki H, et al. (2018). PRC1 Fine-tunes Gene Repression and Activation to Safeguard Skin Development and Stem Cell Specification. Cell Stem Cell 22, 726–739 e727. [PubMed: 29727681]

Cohen I, Zhao D, Menon G, Nakayama M, Koseki H, Zheng D, and Ezhkova E. (2019). PRC1 preserves epidermal tissue integrity independently of PRC2. Genes Dev 33, 55–60. [PubMed: 30567998]

Cooney CA, Jousheghany F, Yao-Borengasser A, Phanavanh B, Gomes T, Kieber-Emmons AM, Siegel ER, Suva LJ, Ferrone S, Kieber-Emmons T, et al. (2011). Chondroitin sulfates play a major role in breast cancer metastasis: a role for CSPG4 and CHST11 gene expression in forming surface P-selectin ligands in aggressive breast cancer cells. Breast Cancer Res 13, R58. [PubMed: 21658254]

Cui R, Widlund HR, Feige E, Lin JY, Wilensky DL, Igras VE, D'Orazio J, Fung CY, Schanbacher CF, Granter SR, et al. (2007). Central role of p53 in the suntan response and pathologic hyperpigmentation. Cell 128, 853–864. [PubMed: 17350573]

Czermin B, Melfi R, McCabe D, Seitz V, Imhof A, and Pirrotta V. (2002). Drosophila enhancer of Zeste/ESC complexes have a histone H3 methyltransferase activity that marks chromosomal Polycomb sites. Cell 111, 185–196. [PubMed: 12408863]

D'Mello SA, Finlay GJ, Baguley BC, and Askarian-Amiri ME (2016). Signaling Pathways in Melanogenesis. Int J Mol Sci 17.

D'Orazio JA, Nobuhisa T, Cui R, Arya M, Spry M, Wakamatsu K, Igras V, Kunisada T, Granter SR, Nishimura EK, et al. (2006). Topical drug rescue strategy and skin protection based on the role of Mc1r in UV-induced tanning. Nature 443, 340–344. [PubMed: 16988713]

Dakup P, and Gaddameedhi S. (2017). Impact of the Circadian Clock on UV-Induced DNA Damage Response and Photocarcinogenesis. Photochem Photobiol 93, 296–303. [PubMed: 27861965]

Dauber KL, Perdigoto CN, Valdes VJ, Santoriello FJ, Cohen I, and Ezhkova E. (2016). Dissecting the Roles of Polycomb Repressive Complex 2 Subunits in the Control of Skin Development. J Invest Dermatol 136, 1647–1655. [PubMed: 26994968]

de Gruijl FR, van Kranen HJ, and Mullenders LH (2001). UV-induced DNA damage, repair, mutations and oncogenic pathways in skin cancer. J Photochem Photobiol B 63, 19–27. [PubMed: 11684448]

de Napoles M, Mermoud JE, Wakao R, Tang YA, Endoh M, Appanah R, Nesterova TB, Silva J, Otte AP, Vidal M, et al. (2004). Polycomb Group Proteins Ring1A/B Link Ubiquitylation of Histone H2A to Heritable Gene Silencing and X Inactivation. Developmental Cell 7, 663–676. [PubMed: 15525528]

del Mar Lorente M, Marcos-Gutierrez C, Perez C, Schoorlemmer J, Ramirez A, Magin T, and Vidal M. (2000). Loss- and gain-of-function mutations show a polycomb group function for Ring1A in mice. Development 127, 5093–5100. [PubMed: 11060235]

Edmondson SR, Russo VC, McFarlane AC, Wraight CJ, and Werther GA (1999). Interactions between growth hormone, insulin-like growth factor I, and basic fibroblast growth factor in melanocyte growth. J Clin Endocrinol Metab 84, 1638–1644. [PubMed: 10323393]

Endoh M, Endo TA, Endoh T, Isono K, Sharif J, Ohara O, Toyoda T, Ito T, Eskeland R, Bickmore WA, et al. (2012). Histone H2A mono-ubiquitination is a crucial step to mediate PRC1-dependent repression of developmental genes to maintain ES cell identity. PLoS Genet 8, e1002774.

Garcia RJ, Ittah A, Mirabal S, Figueroa J, Lopez L, Glick AB, and Kos L. (2008). Endothelin 3 Induces Skin Pigmentation in a Keratin-Driven Inducible Mouse Model. Journal of Investigative Dermatology 128, 131–142.

Goldstein NB, Koster MI, Hoaglin LG, Spoelstra NS, Kechris KJ, Robinson SE, Robinson WA, Roop DR, Norris DA, and Birlea SA (2015). Narrow Band Ultraviolet B Treatment for Human Vitiligo Is Associated with Proliferation, Migration, and Differentiation of Melanocyte Precursors. J Invest Dermatol 135, 2068–2076. [PubMed: 25822579]

Grönniger E, Weber B, Heil O, Peters N, Stäb F, Wenck H, Korn B, Winnefeld M, and Lyko F. (2010). Aging and Chronic Sun Exposure Cause Distinct Epigenetic Changes in Human Skin. PLOS Genetics 6, e1000971.

Hachiya A, Kobayashi A, Ohuchi A, Takema Y, and Imokawa G. (2001). The Paracrine Role of Stem Cell Factor/c-kit Signaling in the Activation of Human Melanocytes in Ultraviolet-B-Induced Pigmentation. Journal of Investigative Dermatology 116, 578–586.

Hachiya A, Sriwiriyanont P, Fujimura T, Ohuchi A, Kitahara T, Takema Y, Kitzmiller WJ, Visscher MO, Tsuboi R, and Boissy RE (2009). Mechanistic effects of long-term ultraviolet B irradiation induce epidermal and dermal changes in human skin xenografts. Am J Pathol 174, 401–413. [PubMed: 19147832]

Harrow J, Frankish A, Gonzalez JM, Tapanari E, Diekhans M, Kokocinski F, Aken BL, Barrell D, Zadissa A, Searle S, et al. (2012). GENCODE: the reference human genome annotation for The ENCODE Project. Genome Res 22, 1760–1774. [PubMed: 22955987]

Huang da W, Sherman BT, and Lempicki RA (2009). Systematic and integrative analysis of large gene lists using DAVID bioinformatics resources. Nat Protoc 4, 44–57. [PubMed: 19131956]

Illingworth RS, Moffat M, Mann AR, Read D, Hunter CJ, Pradeepa MM, Adams IR, and Bickmore WA (2015). The E3 ubiquitin ligase activity of RING1B is not essential for early mouse development. Genes Dev 29, 1897–1902. [PubMed: 26385961]

Katiyar SK, Singh T, Prasad R, Sun Q, and Vaid M. (2012). Epigenetic Alterations in Ultraviolet Radiation-Induced Skin Carcinogenesis: Interaction of Bioactive Dietary Components on Epigenetic Targets†. Photochemistry and Photobiology 88, 1066–1074. [PubMed: 22017262]

Kim M, Han JH, Kim JH, Park TJ, and Kang HY (2016). Secreted Frizzled-Related Protein 2 (sFRP2) Functions as a Melanogenic Stimulator; the Role of sFRP2 in UV-Induced Hyperpigmentary Disorders. J Invest Dermatol 136, 236–244. [PubMed: 26763443]

Knutson SK, Warholic NM, Wigle TJ, Klaus CR, Allain CJ, Raimondi A, Porter Scott M, Chesworth R, Moyer MP, Copeland RA, et al. (2013). Durable tumor regression in genetically altered malignant rhabdoid tumors by inhibition of methyltransferase EZH2. Proc Natl Acad Sci U S A 110, 79227927.

Konze KD, Ma A, Li F, Barsyte-Lovejoy D, Parton T, Macnevin CJ, Liu F, Gao C, Huang XP, Kuznetsova E, et al. (2013). An orally bioavailable chemical probe of the Lysine Methyltransferases EZH2 and EZH1. ACS Chem Biol 8, 1324–1334. [PubMed: 23614352]

Lämke J, and Bäurle I. (2017). Epigenetic and chromatin-based mechanisms in environmental stress adaptation and stress memory in plants. Genome Biology 18, 124. [PubMed: 28655328]

Lee MG, Villa R, Trojer P, Norman J, Yan KP, Reinberg D, Di Croce L, and Shiekhattar R. (2007). Demethylation of H3K27 regulates polycomb recruitment and H2A ubiquitination. Science 318, 447–450. [PubMed: 17761849]

Li M, Indra AK, Warot X, Brocard J, Messaddeq N, Kato S, Metzger D, and Chambon P. (2000). Skin abnormalities generated by temporally controlled RXRα mutations in mouse epidermis. Nature 407, 633636.

Love MI, Huber W, and Anders S. (2014). Moderated estimation of fold change and dispersion for RNA-seq data with DESeq2. Genome Biol 15, 550. [PubMed: 25516281]

Lu Z, Xie Y, Huang H, Jiang K, Zhou B, Wang F, and Chen T. (2020). Hair follicle stem cells regulate retinoid metabolism to maintain the self-renewal niche for melanocyte stem cells. eLife 9, e52712.

Maier K, He Y, Wolfle U, Esser PR, Brummer T, Schempp C, Bruckner-Tuderman L, and Has C. (2016). UV-B-induced cutaneous inflammation and prospects for antioxidant treatment in Kindler syndrome. Hum Mol Genet 25, 5339–5352. [PubMed: 27798104]

Margueron R, and Reinberg D. (2011). The Polycomb complex PRC2 and its mark in life. Nature 469, 343–349. [PubMed: 21248841]

Martens MC, Seebode C, Lehmann J, and Emmert S. (2018). Photocarcinogenesis and Skin Cancer Prevention Strategies: An Update. Anticancer Res 38, 1153–1158. [PubMed: 29374752]

McGrath JA, Robinson MK, and Binder RL (2012). Skin differences based on age and chronicity of ultraviolet exposure: results from a gene expression profiling study. Br J Dermatol 166 *Suppl* 2, 9–15. [PubMed: 22670613]

Moon H, Donahue LR, Choi E, Scumpia PO, Lowry WE, Grenier JK, Zhu J, and White AC (2017). Melanocyte Stem Cell Activation and Translocation Initiate Cutaneous Melanoma in Response to UV Exposure. Cell Stem Cell 21, 665–678 e666. [PubMed: 29033353]

Morris RJ, Liu Y, Marles L, Yang Z, Trempus C, Li S, Lin JS, Sawicki JA, and Cotsarelis G. (2004). Capturing and profiling adult hair follicle stem cells. Nat Biotechnol 22, 411–417. [PubMed: 15024388]

Mu W, Starmer J, Fedoriw AM, Yee D, and Magnuson T. (2014). Repression of the soma-specific transcriptome by Polycomb-repressive complex 2 promotes male germ cell development. Genes Dev 28, 2056–2069. [PubMed: 25228648]

Mull AN, Zolekar A, and Wang YC (2015). Understanding Melanocyte Stem Cells for Disease Modeling and Regenerative Medicine Applications. Int J Mol Sci 16, 30458–30469. [PubMed: 26703580]

Murase D, Hachiya A, Amano Y, Ohuchi A, Kitahara T, and Takema Y. (2009). The essential role of p53 in hyperpigmentation of the skin via regulation of paracrine melanogenic cytokine receptor signaling. J Biol Chem 284, 4343–4353. [PubMed: 19098008]

Nguyen NT, and Fisher DE (2019). MITF and UV responses in skin: From pigmentation to addiction. Pigment Cell & Melanoma Research 32, 224–236. [PubMed: 30019545]

Nowak JA, and Fuchs E. (2009). Isolation and culture of epithelial stem cells. Methods Mol Biol 482, 215–232. [PubMed: 19089359]

Palmieri G, Ombra M, Colombino M, Casula M, Sini M, Manca A, Paliogiannis P, Ascierto PA, and Cossu A. (2015). Multiple Molecular Pathways in Melanomagenesis: Characterization of Therapeutic Targets. Frontiers in Oncology 5.

Perdigoto CN, Valdes VJ, Bardot ES, and Ezhkova E. (2012). Epigenetic regulation of skin: focus on the Polycomb complex. Cell Mol Life Sci 69, 2161–2172. [PubMed: 22314499]

Qiu W, Chuong CM, and Lei M. (2019). Regulation of melanocyte stem cells in the pigmentation of skin and its appendages: Biological patterning and therapeutic potentials. Exp Dermatol 28, 395–405. [PubMed: 30537004]

Qutob SS, Chauhan V, Kuo B, Williams A, Yauk CL, McNamee JP, and Gollapudi B. (2018). The application of transcriptional benchmark dose modeling for deriving thresholds of effects associated with solar-simulated ultraviolet radiation exposure. Environ Mol Mutagen 59, 502–515. [PubMed: 29761935]

Schadendorf D, van Akkooi ACJ, Berking C, Griewank KG, Gutzmer R, Hauschild A, Stang A, Roesch A, and Ugurel S. (2018). Melanoma. The Lancet 392, 971–984.

Schuettengruber B, Bourbon H-M, Di Croce L, and Cavalli G. (2017). Genome Regulation by Polycomb and Trithorax: 70 Years and Counting. Cell 171, 34–57. [PubMed: 28938122]

Simon JA, and Kingston RE (2009). Mechanisms of Polycomb gene silencing: knowns and unknowns. Nature Reviews Molecular Cell Biology 10, 697–708. [PubMed: 19738629]

Simon JA, and Kingston RE (2013). Occupying chromatin: Polycomb mechanisms for getting to genomic targets, stopping transcriptional traffic, and staying put. Mol Cell 49, 808–824. [PubMed: 23473600]

Strub T, Ghiraldini FG, Carcamo S, Li M, Wroblewska A, Singh R, Goldberg MS, Hasson D, Wang Z, Gallagher SJ, et al. (2018). SIRT6 haploinsufficiency induces BRAF(V600E) melanoma cell resistance to MAPK inhibitors via IGF signalling. Nat Commun 9, 3440. [PubMed: 30143629]

Tanimura S, Tadokoro Y, Inomata K, Binh NT, Nishie W, Yamazaki S, Nakauchi H, Tanaka Y, McMillan JR, Sawamura D, et al. (2011). Hair Follicle Stem Cells Provide a Functional Niche for Melanocyte Stem Cells. Cell Stem Cell 8, 177–187. [PubMed: 21295274]

Timpl R, Sasaki T, Kostka G, and Chu M-L (2003). Fibulins: a versatile family of extracellular matrix proteins. Nature Reviews Molecular Cell Biology 4, 479–489. [PubMed: 12778127]

Valejo Coelho MM, Matos TR, and Apetato M. (2016). The dark side of the light: mechanisms of photocarcinogenesis. Clinics in Dermatology 34, 563–570. [PubMed: 27638434]

Wang H, Wang L, Erdjument-Bromage H, Vidal M, Tempst P, Jones RS, and Zhang Y. (2004). Role of histone H2A ubiquitination in Polycomb silencing. Nature 431, 873–878. [PubMed: 15386022]

Wang W, Qin J-J, Voruganti S, Nag S, Zhou J, and Zhang R. (2015). Polycomb Group (PcG) Proteins and Human Cancers: Multifaceted Functions and Therapeutic Implications. Med Res Rev 35, 1220–1267. [PubMed: 26227500]

Xu Z, Chen L, Jiang M, Wang Q, Zhang C, and Xiang LF (2018). CCN1/Cyr61 Stimulates Melanogenesis through Integrin alpha6beta1, p38 MAPK, and ERK1/2 Signaling Pathways in Human Epidermal Melanocytes. J Invest Dermatol 138, 1825–1833. [PubMed: 29510193]

Zhang J, Zhang J, Wang F, Xu X, Li X, Guan W, Men T, and Xu G. (2021). Overexpressed COL5A1 is correlated with tumor progression, paclitaxel resistance, and tumor-infiltrating immune cells in ovarian cancer. J Cell Physiol.

Zhang YV, White BS, Shalloway DI, and Tumbar T. (2010). Stem cell dynamics in mouse hair follicles: a story from cell division counting and single cell lineage tracing. Cell Cycle 9, 1504–1510. [PubMed: 20372093]

Zhao D, and Zheng D. (2018). SMARTcleaner: identify and clean off-target signals in SMART ChIP-seq analysis. BMC Bioinformatics 19, 544. [PubMed: 30587107]

Highlights

- Polycomb repression is reduced in the epidermis upon low-dose UV exposure.
- Loss of Polycomb repression in the epidermis results in epidermal pigmentation.
- Polycomb controls epidermal pigmentation via a p53-independent pathway.
- Type II collagen promotes UV-induced epidermal pigmentation.

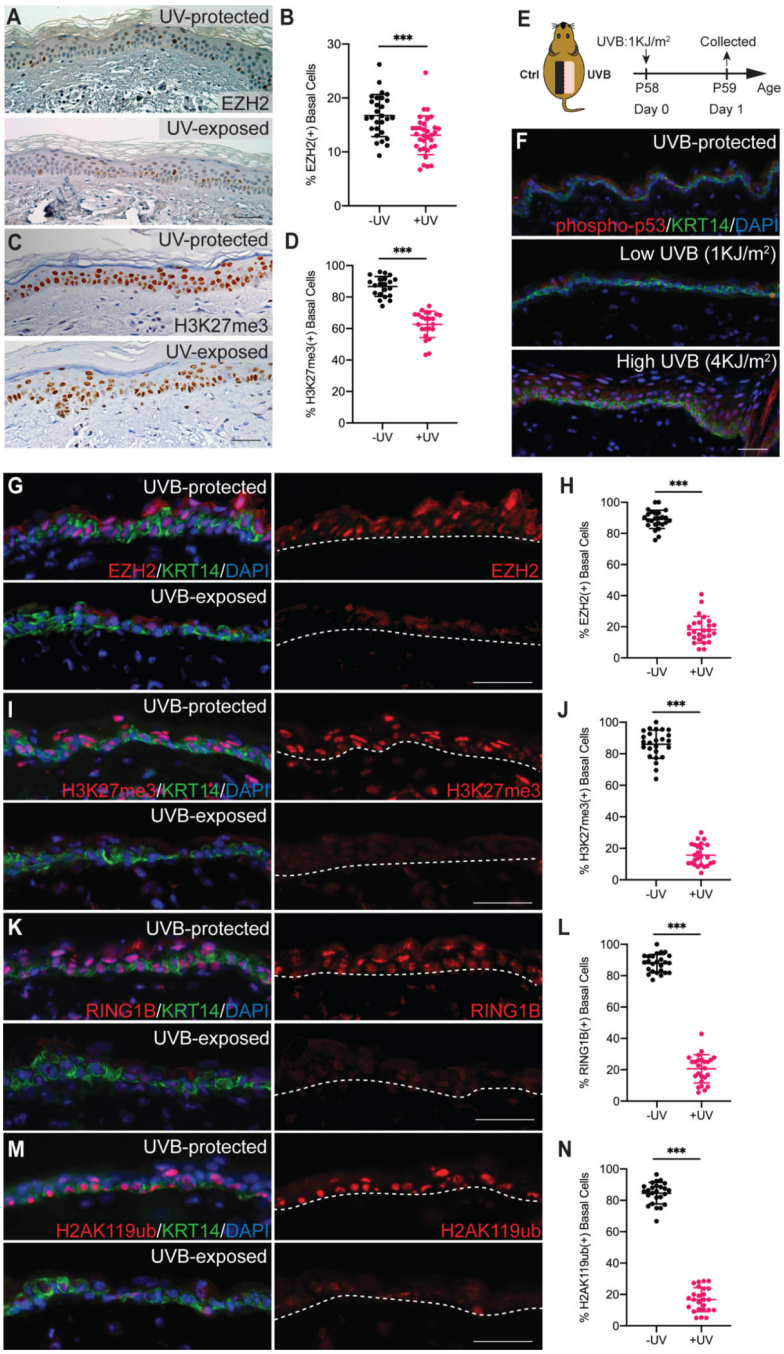

Figure 1. Function of PRC1 and PRC2 diminishes upon UVB exposure in human and mouse epidermis.

(A) Immunohistochemistry (IHC) analysis of EZH2 in UV-protected and UV-exposed human epidermis. **(B)** Quantifications of EZH2 positive (+) cells in the basal layer of the epidermis. ***p-value < 0.001; n = 5, UV-protected skin; n = 7, UV-exposed skin. **(C)** IHC analysis of H3K27me3 in UV-protected and UV-exposed human skin. **(D)** Quantifications of H3K27me3(+) cells in the basal layer. ***p-value < 0.001; n = 4, UV-protected skin; n = 5, UV-exposed skin. **(E)** UVB irradiation experimental design. See text and STAR methods

for details. **(F)** Immunofluorescence (IF) analysis of phospho-p53 (red) and basal epithelial marker keratin 14 (KRT14) (green) in UVB-protected, low UVB (1KJ/m^2)-exposed and high UVB (4KJ/m^2)-exposed skins. **(G–N)** IF analysis of EZH2 (G; red), H3K27me3 (I; red), RING1B (K; red), H2AK119ub (M; red) and basal epithelial marker KRT14 (green) in skins of UVB-protected and UVB-irradiated mice. Quantifications of EZH2 (H), H3K27me3 (J), RING1B (L), and H2AK119ub (N) positive cells in the basal layer. ***p-value < 0.001; n = 3, UV-protected mice; n = 3, UV-exposed mice. Scale bars of IF and brightfield images are 50 μm. Data in (B, D, H, J, L, N) are mean ± SD.

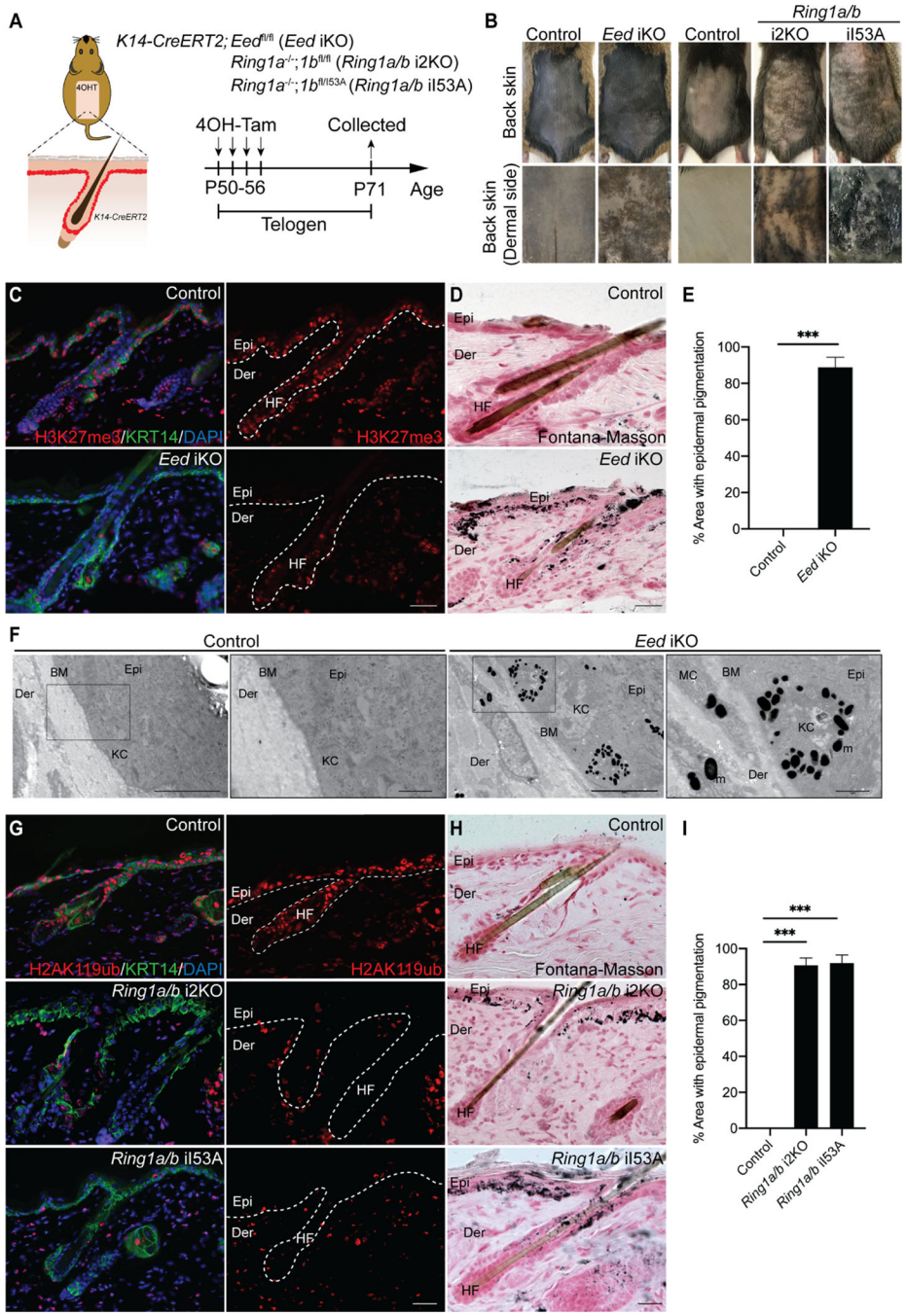

Figure 2. Loss of canonical PRC1 and PRC2 function leads to epidermal hyperpigmentation.

(A) Treatment strategy of inducing conditional PRC1 and PRC2 knockout mice. See text and STAR methods for details. **(B)** Macroscopic skin hyperpigmentation phenotype (top) and representative images of dermal side of back skin depicting hyperpigmentation (bottom) in P71 control, *Eed* iKO, *Ring1a/b* i2KO, and *Ring1a/b* iI53A mice. **(C)** IF analysis of H3K27me3 (red) and basal epithelial marker KRT14 (green) in P71 control and *Eed* iKO back skin sections. **(D)** Fontana-Masson staining of P71 control and *Eed* iKO back skin sections. Melanin pigment is in black. **(E)** Quantification of epidermal pigmentated areas

in P71 control and *Eed* iKO back skin sections. ***p-value < 0.001; n = 3 animals per genotype. **(F)** Transmission Electron Microscopy (TEM) analysis of melanosomes in P71 control and *Eed* iKO epidermis. Melanosomes (m) are presented in the keratinocytes (KC) and melanocytes (MC). Scale bar, 10 μm. Magnified view of enclosed area is to the right of each image. Scale bar, 1 μm. **(G)** IF analysis of H2AK119ub (red) and KRT14 (green) in P71 control, *Ring1a/b* i2KO, and *Ring1a/b* iI53A back skin sections. **(H)** Fontana-Masson staining in P71 control, *Ring1a/b* i2KO, and *Ring1a/b* iI53A back skin sections. **(I)** Quantification of epidermal pigmentated areas in P71 control, *Ring1a/b* i2KO, and *Ring1a/b* iI53A back skin sections. ***p-value < 0.001; n = 3 animals per genotype. Epi, epidermis; Der, dermis; HF, hair follicle; BM, basement membrane. Scale bars in IF and bright-field images, 50 μm. White dashed lines outline the epidermis and the hair follicle areas. Data in (E, I) are mean ± SD.

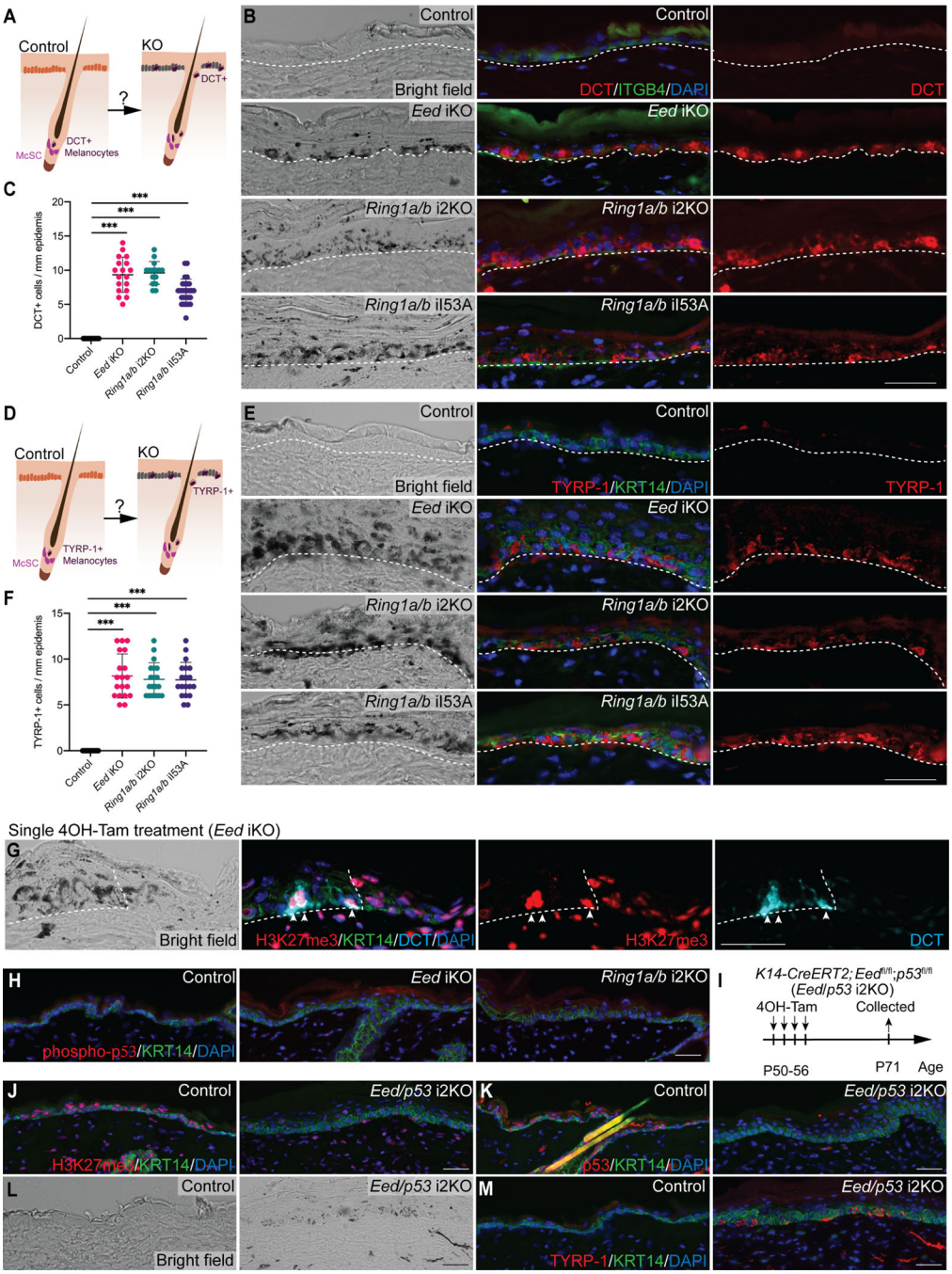

Figure 3. Loss of canonical PRC1 and PRC2 function results in the presence of differentiated melanocytes in the interfollicular epidermis.

(A, D) Illustration of the hypothesis that loss of canonical Polycomb function leads to the presence of melanocyte marker DCT(+) (A) and TYRP-1(+) (D) melanocytes in the interfollicular epidermis (IFE), which are normally present only in hair follicles. **(B)** Bright-field and IF analysis of melanocyte marker DCT (red) and basement membrane marker Integrin β4 (ITGB4; green) in P71 control, *Eed* iKO, *Ring1a/b* i2KO, and *Ring1a/b* iI53A back skins. White dashed lines outline the epidermis–dermis borders. **(C)** Quantification of

DCT(+) melanocytes in the IFE of P71 control and Polycomb mutant skin. ***p-value < 0.001; n = 4 animals per genotype. **(E)** Bright-field and IF analysis of melanocyte marker TYRP-1 (red) and basal epithelial marker KRT14 (green) of P71 control, *Eed* iKO, *Ring1a/b* i2KO, and *Ring1a/b* iI53A. White dashed lines outline the epidermis–dermis borders. **(F)** Quantification of TYRP-1(+) melanocytes in the IFE of P71 control and Polycomb mutant skin. ***p-value < 0.001; n = 4 animals per genotype. **(G)** Bright-field and IF analysis of H3K27me3 (red), KRT14 (green), and DCT (cyan) staining in the back skin of mice treated with a single dose 4OH-Tam to induce mosaic *Eed*-null clones in the epidermis. Dashed lines outline the border of the *Eed*-null clone. White arrowheads indicate melanocytes in the epidermis. **(H)** IF analysis of phospho-p53 (red) and KRT14 (green) in P71 control, *Eed* iKO, and *Ring1a/b* i2KO dorsal skin sections**. (I)** Experimental design for topical treatment of P50 control and *K14CreERT2*; $Eed^{fl/fl}$; $p53^{fl/fl}$ (*Eed/p53* iKO) mice. See details in STAR methods. **(J–K)** IF analysis of H3K27me3 (J; red), p53 (K; red) and KRT14 (green) in P71 control and *Eed/p53* i2KO back skins. **(L)** Bright-field images (left) and IF analysis of TYRP-1 (right; red) and KRT14 (green) of P71 control and *Eed/p53* i2KO back skins. Scale bars, 50 μm. Data in (C, F) are mean ± SD.

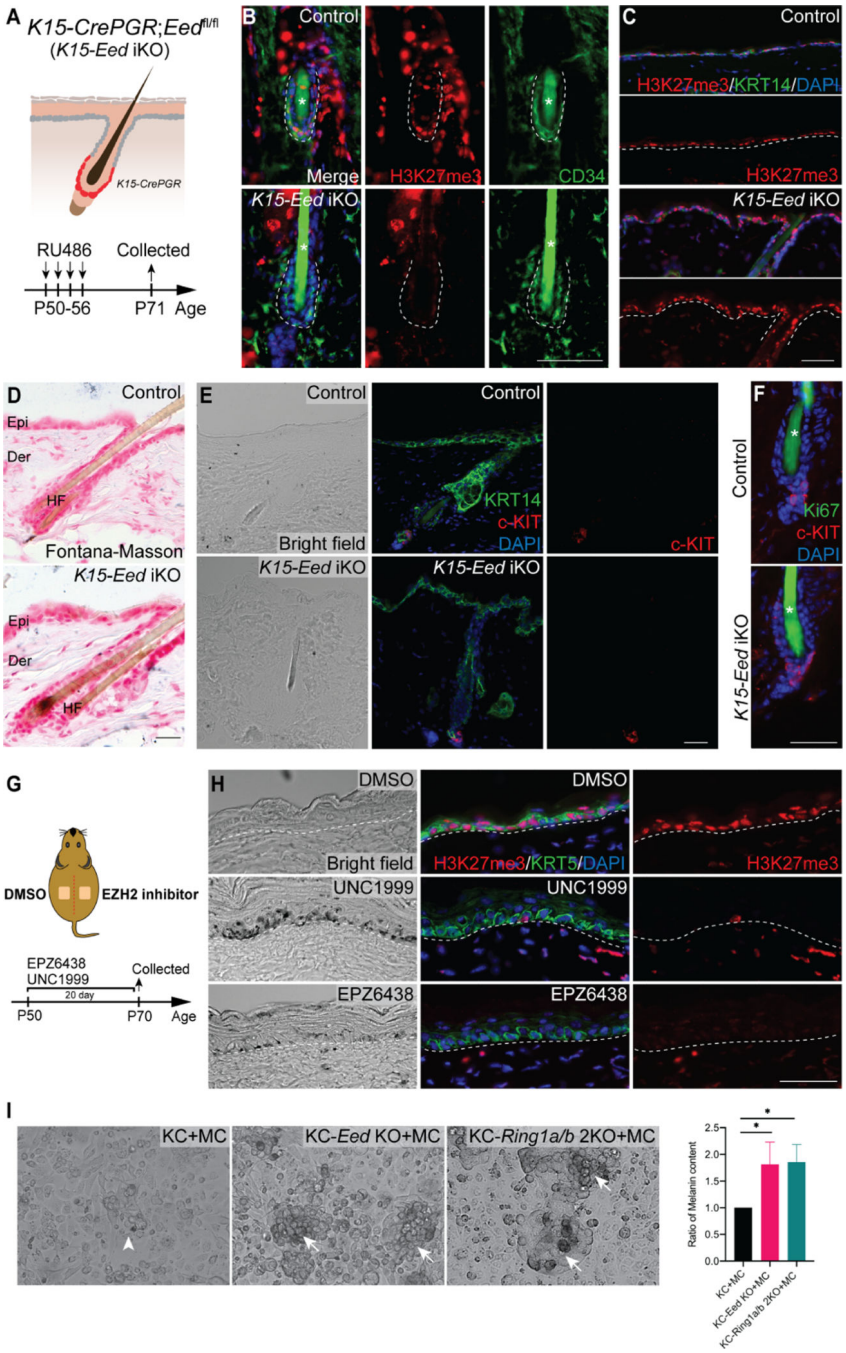

Figure 4. Loss of PRC2 in hair follicle stem cells does not induce epidermal pigmentation.

(A) Experimental design for topical treatment of P50 control and *K15-CrePGR*; *Eed*$^{fl/fl}$ (*K15-Eed* iKO) mice with RU-486. See details in STAR methods. **(B)** IF analysis of H3K27me3 (red) and hair follicle stem cell marker CD34 (green) in the bulge area of P71 control and *K15-Eed* iKO mice. **(C)** IF analysis of H3K27me3 (red) and basal epithelial marker KRT14 (green) in the epidermis of P71 control and *K15-Eed* iKO mice. White dashed lines outline the bulge–dermis border (B) and epidermis–dermis border (C). **(D)** Fontana-Masson staining of P71 control and *K15-Eed* iKO back skin sections. Melanin

pigment staining is black. **(E)** Bright-field and IF analysis of melanocyte marker c-KIT (red) and KRT14 (green) staining in the hair follicles and epidermis of P71 control and *K15-Eed* iKO mice. **(F)** IF analysis of c-KIT (red) and proliferation marker Ki67 (green) in the bulge area of P71 control and *K15-Eed* iKO mice. **(G)** Experimental design for topical treatment of back skin of P50 wild-type mice with EZH2 inhibitors. See details in STAR methods. **(H)** Bright-field and IF analysis of H3K27me3 (red) and basal epithelial marker keratin 5 (KRT5; green) of P71 back skin of mice treated with EZH2 inhibitors (UNC1999 and EPZ6438). White dashed lines outline the epidermis–dermis border. **(I)** Left, bright-field images of control EpSCs (KC), *Eed*-null EpSCs (KC-*Eed* KO), or *Ring1a/b*-null EpSCs (KC-*Ring1a/b* 2KO) co-cultured with B16F0 melanocytes (MC) for 72 h. Right, quantification of melanin content in control KC-MC, KC-*Eed* KO-MC, and KC-*Ring1a/b* 2KO-MC co-cultures, *p-value < 0.05; n = 3 replicates per group. Data are mean ± SD. White arrowheads indicate melanocytes in the control co-culture. White arrows indicate melanocytes in Polycomb mutant co-cultures. Asterisks indicate autofluorescence in the hair shaft. Scale bars, 50 μm.

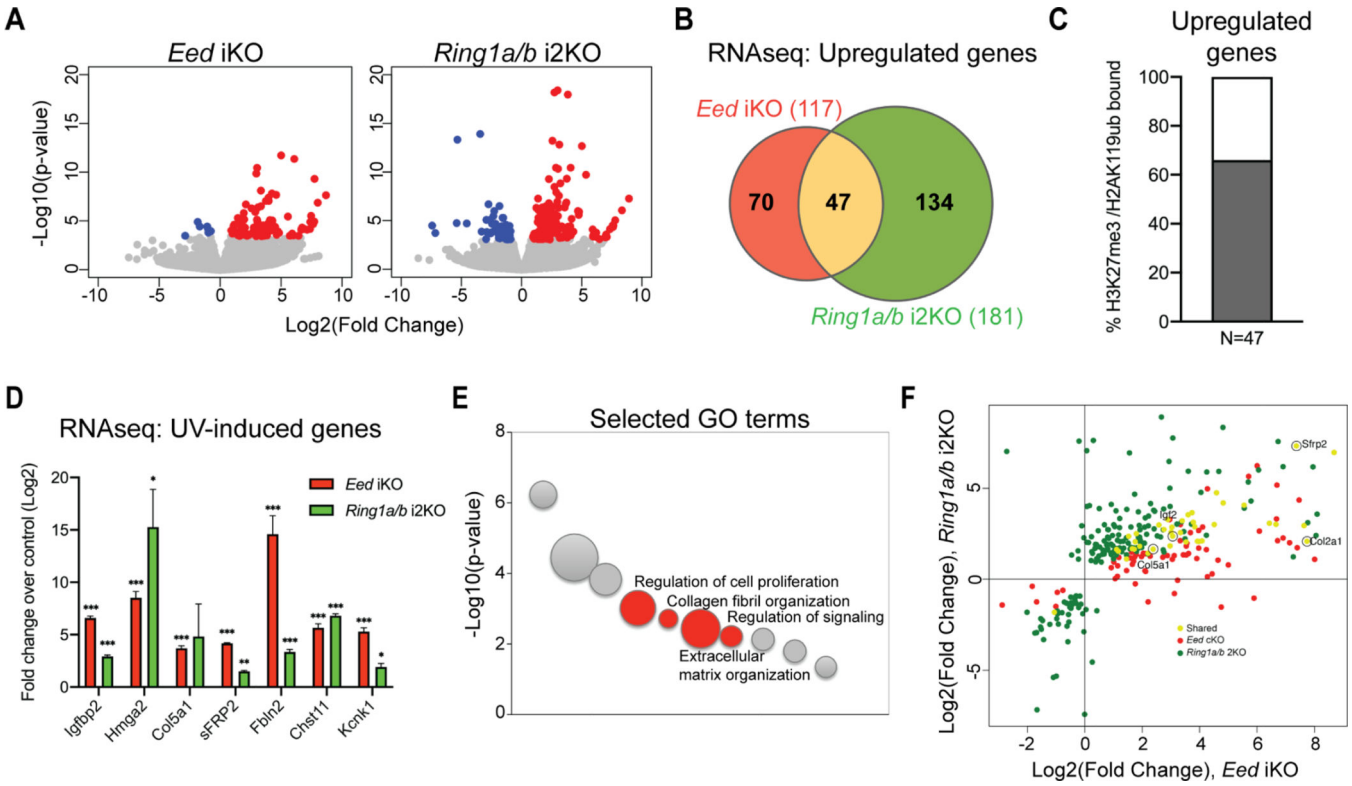

Figure 5. Genes encoding extracellular matrix organization components are upregulated in PRC1 and PRC2-null epidermis.

(A) Differentially expressed genes in FACS-purified *Eed* iKO EpSCs (left) and *Ring1a/b* i2KO EpSCs (right) vs. corresponding controls. Genes with absolute fold change ≥ 2 and adjusted p-value < 0.05 were considered upregulated (red) or downregulated (blue). **(B)** Venn diagram showing the overlap of significantly upregulated genes in *Eed* iKO EpSCs (117 genes) and *Ring1a/b* i2KO EpSCs (181 genes). **(C)** Percentage of genes upregulated in *Eed* iKO and *Ring1a/b* i2KO (47 genes) demarcated by both H3K27me3 and H2AK119ub. **(D)** qPCR analysis of UVB-induced genes that are directly targeted by PRC1 and PRC2 and upregulated in *Eed* iKO and *Ring1a/b* i2KO. n = 3 in *Eed* iKO and n = 2 in *Ring1a/b* i2KO. ***p-value < 0.001, **p-value < 0.01, *p-value < 0.05; Data are mean ± SD. **(E)** Gene ontology (GO) analysis of genes upregulated in *Eed* iKO and *Ring1a/b* i2KO EpSCs. Selected GO terms are labeled in red. **(F)** Expression of selected genes in *Eed* iKO (red) and *Ring1a/b* i2KO (green). Genes upregulated in both mutants are labeled in yellow.

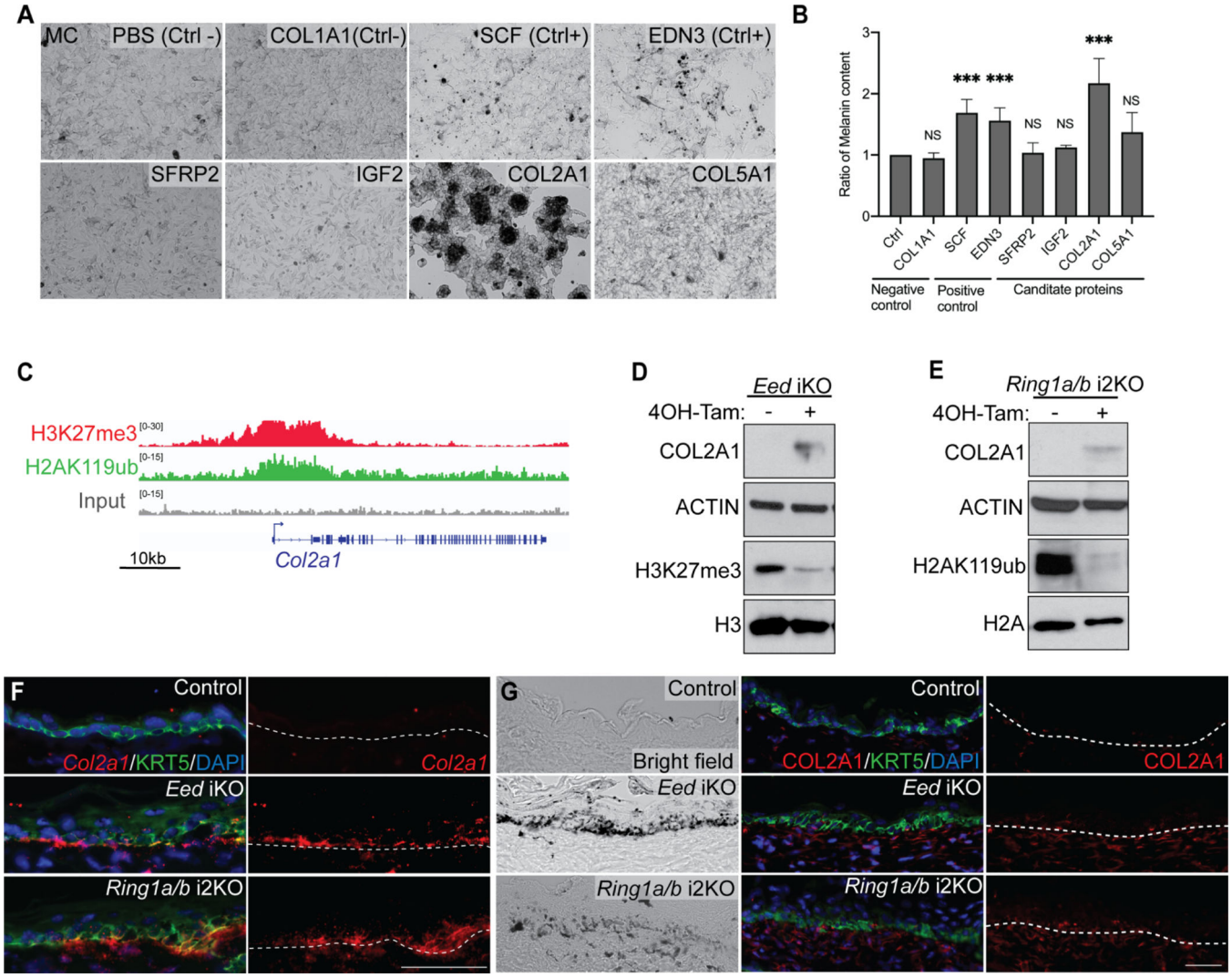

Figure 6. Loss of PRC1 and PRC2 leads to upregulation of type II collagen in EpSCs, resulting in epidermal pigmentation.

(A) *In vitro* pigmentation assay: melanocytes cultured on wells precoated with different proteins to test melanin production. Cells cultured on wells precoated with PBS or type I collagen (COL1A1) are negative controls (Ctrl-). Cells cultured on wells with SCF or EDN3 are positive controls (Ctrl+). **(B)** Quantification of melanin content normalized to PBS controls. NS, not significant; ***p-value < 0.001; n = 3 replicates per group. Data are mean ± SD. **(C)** Integrative genomics viewer (IGV) tracks of H3K27me3, H2AK119ub, and input for the *Col2a1* locus. Arrows indicate the transcription start site (TSS). **(D–E)** Western blot analyses of control, *Eed* iKO (D), and *Ring1a/b* i2KO (E) EpSCs with antibodies as indicated. **(F)** *In situ* hybridization/IF analysis of *Col2a1* RNA (red) and basal epithelial marker KRT5 (green) of P71 control, *Eed* iKO, and *Ring1a/b* i2KO back skin sections. **(G)** Bright-field and IF analysis of type II collagen (COL2A1; red) and KRT5 (green) of P71 control, *Eed* iKO, and *Ring1a/b* i2KO back skin sections. White dashed lines outline the epidermis–dermis borders. Scale bars, 50 μm.

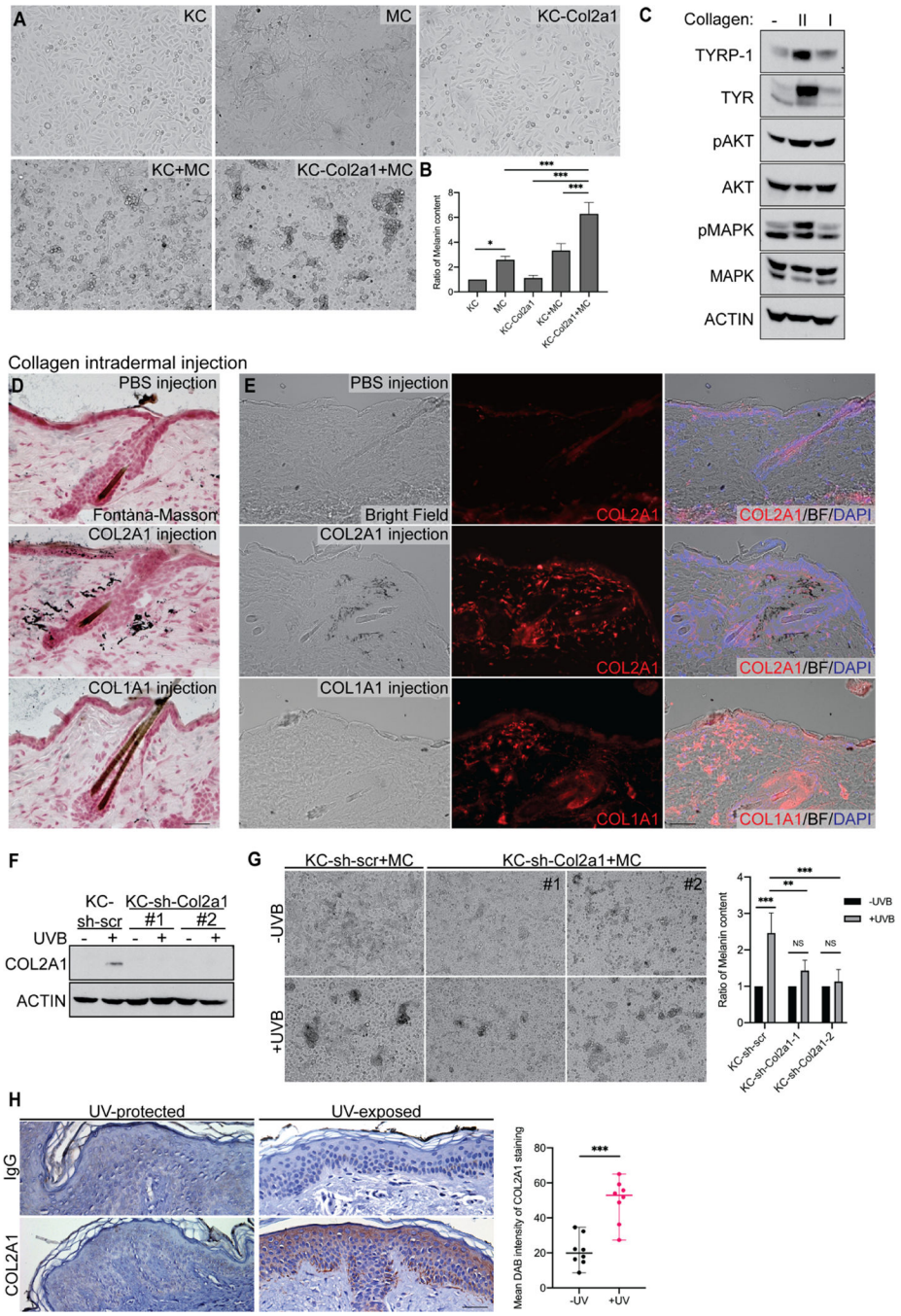

Figure 7. Type II collagen promotes epidermal pigmentation *in vitro* and *in vivo*.

(A) Co-culturing assay of control EpSCs (KC) or EpSCs expressing type II collagen (KC-Col2a1) co-cultured with or without B16F0 melanocytes (MC). **(B)** Quantification of melanin content in co-culture assays presented in (A). * p-value < 0.05, ***p-value < 0.001; n = 3 replicates per group. **(C)** Western blot analysis of B16F0 melanocytes (MC) cultured on control (−), type II collagen (II), and type I collagen (I)-coated plates with antibodies as indicated. **(D)** Fontana-Masson staining of P71 mice intradermally injected with PBS, COL2A1, or COL1A1. Melanin pigment is in black. **(E)** Bright-field (BF) and IF analysis of

COL2A1 (red) or COL1A1 (red) in the back skin of mice intradermally injected with PBS, COL2A1, or COL1A1. **(F)** Western blot analysis of EpSCs expressing scrambled shRNA control (KC-sh-scr) or 2 different shRNAs targeting *Col2a1* (KC-sh-Col2a1 #1 and #2) 5 days post UVB irradiation with antibodies as indicated. **(G)** Representative images (left) and quantification of melanin content (right) in KC infected with sh-scr, sh-Col2a1–1, or sh-Col2a1–2 co-cultured with MC and with (lower panel) or without (upper panel) UVB exposure. **p-value < 0.01, ***p-value < 0.001; n = 6 replicates per group. **(H)** IHC staining of type II collagen (COL2A1) and IgG (negative control) in UV-protected and UV-exposed human skin (left). Quantification of mean DAB intensity of COL2A1 expression in UV-protected and UV-exposed human skin samples (right). ***p-value < 0.001; n = 8 replicates per group. Data in (B, G, H) are mean ± SD. Scale bars, 50 μm.

KEY RESOURCES TABLE

REAGENT or RESOURCE	SOURCE	IDENTIFIER
Antibodies		
Rabbit anti-H2AK119ub	Cell Signaling	Cat # 8240s
Rabbit anti-H3K27me3	MilliporeSigma	Cat # 07-449, RRID: AB_310624
Chicken anti-Keratin 5	BioLegend	Cat # 905901, RRID: AB_2565054
Chicken anti-Keratin 14	BioLegend	Cat # 906001, RRID: AB_2565055
Rat anti-Itgb4 (CD104)	BD Biosciences	Cat # 553745, RRID: AB_395027
Rabbit anti-Ki67	Abcam	Cat # ab15580, RRID: AB_443209
Rabbit anti-EZH2	Cell Signaling	Cat # 5264s
Mouse anti-EZH2	BD Biosciences	Cat # 612667, RRID: AB_399911
Goat anti-DCT	Santa Cruz Biotechnology	Cat # sc-10451, RRID: AB_793582
Rabbit anti-TYRP1	Novus	Cat # NBP1-88370, RRID: AB_11004292
Rabbit anti-TYR	ABclonal	Cat # A1254, RRID: AB_2759379
Mouse-anti-RING1B	Active Motif	Cat # 39663, AB_2615006
Rabbit-anti-RING1B	Cell Signaling	Cat # 5694s
Rabbit anti-c-KIT (CD117)	Cell Signaling	Cat # 3074s
Rat anti-c-KIT (CD117)	BioLegend	Cat # 135104, RRID: AB_1877057
Rabbit anti-COL2A1	Abcam	Cat # ab34712, RRID: AB_731688
Rabbit anti-COL1A1	ABclonal	Cat # A1352, RRID: AB_2760381
Mouse anti-ACTIN	Sigma-Aldrich	Cat # A5316, RRID: AB_476743
Rabbit anti-H3	Abcam	Cat # ab1791, RRID: AB_30261
Rabbit anti-H2A	Abcam	Cat # ab18255, RRID: AB_470265
Mouse anti-CD34	Thermo Fisher Scientific	Cat # 14-0341-82, RRID: AB_467210
Rabbit anti-Caspase 3	R&D Systems	Cat # AF835, RRID: AB_2243952
Rabbit anti-γH2AX	MilliporeSigma	Cat # 05-636, RRID: AB_309864
Rabbit IgG	MilliporeSigma	Cat # PP64, RRID:AB_97852
Rabbit anti-Phospho-p53 (Ser9)	Cell Signaling	Cat # 9288
Rabbit anti-p53 antibody	Cell Signaling	Cat # 9282
Rabbit anti-Phospho-MAPK	Cell Signaling	Cat # 9101S
Rabbit anti-MAPK	Cell Signaling	Cat # 9102S
Rabbit anti-Phospho-AKT (Ser473)	Cell Signaling	Cat # 4060
Rabbit anti-AKT	Cell Signaling	Cat # 9272
Rabbit anti-CD3	BioLegend	Cat # 100212, RRID: AB_493530
Rat anti-mouse Ly-6G	BioLegend	Cat # 127636, RRID: AB_2563207
APC anti-mouse CD326 (Epcam)	BioLegend	Cat # 118214, RRID: AB_1134102
PerCP-Cyanine5.5 anti-mouse Sca-1	Thermo Fisher Scientific	Cat # 45-5981-82, RRID: AB_914372
FITC anti-CD49f (Integrin alpha 6)	Thermo Fisher Scientific	Cat # 11-0495-82, RRID: AB_11150059
Anti-Rabbit Alexa Fluor 488	Jackson ImmunoResearch Labs	Cat # 711-545-152, RRID: AB_2313584

REAGENT or RESOURCE	SOURCE	IDENTIFIER
Anti-Rabbit Alexa Fluor 594	Jackson ImmunoResearch Labs	Cat # 711-585-152, RRID: AB_2340621
Anti-Rat Alexa Fluor 488	Jackson ImmunoResearch Labs	Cat # 712-545-150, RRID: AB_2340683
Anti-Rat Alexa Fluor 594	Jackson ImmunoResearch Labs	Cat # 712-585-150, RRID: AB_2340688
Anti-Goat Rhodamine Red-X	Jackson ImmunoResearch Labs	Cat # 705-295-147, RRID: AB_2340423
Anti-Goat Alexa Fluor 647	Jackson ImmunoResearch Labs	Cat # 705-606-147, RRID: AB_2340438
Anti-Chicken Alexa Fluor 488	Jackson ImmunoResearch Labs	Cat # 703-545-155, RRID: AB_2340375
4′,6-Diamidino-2-phenylindole dihydrochloride (DAPI)	Sigma-Aldrich	Cat # 32670
HRP anti-Rabbit IgG	Jackson ImmunoResearch Labs	Cat # 711-035-152 RRID: AB_10015282
HRP anti-Mouse IgG	Jackson ImmunoResearch Labs	Cat # 115-036-075 RRID: AB_2338526
Chemicals, Peptides, and Recombinant Proteins		
Pierce 16% Formaldehyde (w/v), Methanol-free	Thermo Fisher Scientific	Cat # 28906
Glutaraldehyde 50%, EM grade	Electron Microscopy Sciences	Cat # 16320
Type II Collagen from chicken sternal cartilage	Sigma-Aldrich	Cat # C9301
Type I Collagen from rat tail	Sigma-Aldrich	Cat # C7661
Type V Collagen from human placenta	Sigma-Aldrich	Cat # C3657
Recombinant Human SCF Protein	R&D Systems	Cat # 7466-SC
Recombinant Human Endothelin-3 Protein	R&D Systems	Cat # NBP2-51961
Recombinant human sFRP-2 protein	R&D Systems	Cat # 6838-FR
Recombinant Mouse IGF-II/IGF2 Protein	R&D Systems	Cat # 792-MG
Dimethyl sulfoxide (DMSO)	Sigma-Aldrich	Cat # D4540
4-Hydroxytamoxifen	Sigma-Aldrich	Cat # H6278
Mifepristone (RU486)	Cayman chemicals	Cat # 10006317
EPZ6438	This paper	N/A
UNC1999	This paper	N/A
Tissue-Tek® O.C.T. Compound	Sakura	Cat # 4583
Trypsin EDTA (0.25%) phenol red	Gibco	Cat # 25200-056
DPBS (without Ca and Mg)	Corning	Cat # 21-031-CV
DMEM	Corning	Cat # 10-013-CV
Fetal Bovine Serum	R&D Systems	Cat # S11550
Donkey Serum	Sigma-Aldrich	Cat # S30
Penicillin-Streptomycin Solution, 100x	Corning	Cat # 30-002-CI
Mitomycin C	Roche	Cat # 10107409001
E media	Nowak and Fuchs, 2009	N/A
Penicillin-Streptomycin	Corning	Cat # 30-002-Cl
Dimethyl sulfoxide	Sigma-Aldrich	Cat # D4540
Polybrene	Sigma-Aldrich	Cat # H9268
Blasticidin S	Sigma-Aldrich	Cat # SBR00022
Puromycin	Sigma-Aldrich	Cat # P8833
RNase A	Thermo Fisher Scientific	Cat # EN0531

REAGENT or RESOURCE	SOURCE	IDENTIFIER
Proteinase K	Roche	Cat # 3115879001
Propylene oxide	Electron Microscopy Sciences	Cat # 20412
The Taab 812 Resin	TAAB laboratory and microscopy	Cat # T022
Osmium Tetroxide-2% solution	Electron Microscopy Sciences	Cat # 19150
Hair remover lotion	Nair©	N/A
Ethanol, Absolute (200 Proof)	Thermo Fisher Scientific	Cat # BP2818
RNAscope® Probe - Mm-Col2a1	Advanced Cell Diagnostics	Cat # 407221
MG132	Selleckchem	Cat # S2619
Critical Commercial Assays		
Zombie Violet Fixable Viability Kit	BioLegend	Cat # 423113
RNeasy Plus Micro Kit	QIAGEN	Cat # 74034
RNase-free DNase Kit	QIAGEN	Cat # 79254
qScript cDNA SuperMix	Quanta	Cat # 95048
LightCycler® 480 SYBR Green I Master mix	Roche	Cat # 04707516001
Ovation® RNA-Seq V2 plus Ultralow	NuGEN	Cat # 0505NB
Agencourt AMPure XP	Beckman Coulter	Cat # A63880
Dynabeads protein G	Invitrogen	Cat # 10004D
ChIP DNA Clean and Concentrator kit	Zymo Research	Cat # D5205
NEBNext® Multiplex Oligos for Illumina®	New England Biolabs	Cat # E7335S
NEBNext® Ultra™ II DNA Library Prep Kit for Illumina®	New England Biolabs	Cat # E7645S
ImmPRESS® HRP Anti-Mouse IgG (Peroxidase) Polymer Detection Kit	VECTOR Laboratories	Cat # MP-7402-15
ImmPRESS® HRP Anti-Rabbit IgG (Peroxidase) Polymer Detection Kit	VECTOR Laboratories	Cat # MP-7401-15
ImmPACT® DAB Peroxidase (HRP) Substrate	VECTOR Laboratories	Cat # SK-4105
Fontana-Masson Stain Kit	Sigma-Aldrich	Cat # HT200
DirectPCR (yolk sac)	Viagen Biotech	Cat # 202-y
cOmplete™ Protease Inhibitor Cocktail	Roche	Cat # 11697498001
UVB lamp	OSRAM	Cat # P10650009
UVP Blak-Ray Lamp XX-15MR	Analytik Jena	Cat # 95-0042-08
UV513AB Digital UVA/UVB Meter	General Tools	Cat # UV513AB
jetPEI®, HTS DNA transfection reagent	Polyplus-transfection	Cat # 89129-916
RNAscope® 2.5 HD Reagent Kit-RED	Advanced Cell Diagnostics	Cat # 322350
RNAscope® Protease III and IV Reagents	Advanced Cell Diagnostics	Cat # 322340
Experimental Models: Organisms/Strains		
Mouse: C57BL/6J	Jackson Labs	000664
Mouse: *K14-CreERT2*	Li *et al.*, 2000, Zhang *et al.*, 2000	N/A
Mouse: *K15-CrePR*	Jackson Labs	005249
Mouse: $Eed^{flox/flox}$	Mu *et al.*, 2014	N/A
Mouse: $Ring1a^{-/-}$	del Mar *et al.*, 2000	N/A

REAGENT or RESOURCE	SOURCE	IDENTIFIER
Mouse: *Ring1b*$^{flox/flox}$	Calés *et al.*, 2008	N/A
Mouse: *Ring1b*^{I53A}	Illingworth *et al.,* 2015	N/A
Mouse: *p53*^{LoxP}	Jackson Labs	008462
Mouse: *Tyr-CreERT2*	Jackson Labs	012328
Mouse: *Rosa*^{mTmG}	Jackson Labs	007676
Recombinant DNA		
pLX304-Col2a1	Horizon Discovery lentiviral library	CCSB-Broad Lentiviral Expression Clones (OHS6085)
pMD2.G	Addgene	#12259
psPAX2	Addgene	#12260
Experimental Models: Cell Lines		
Mouse*: K14-CreERT*; *Ring1a*$^{-/-}$*;Ring1b*$^{flox/flox}$ EpSCs culture	Cohen *et al.*, 2018	N/A
Mouse: *K14-CreERT2*; *Eed*$^{flox/flox}$ EpSCs culture	This paper	N/A
B16F0	ATCC®	Cat # CRL-6322
Deposited Data		
ChIP-seq data	This paper	GEO: GSE159767
RNA-seq data	This paper	GEO: GSE159767
Oligonucleotides		
Primers for mouse genotyping, see Table S3	This paper	N/A
Primers for RT-qPCR, see Table S3	This paper	N/A
pLKO-Col2a1-shRNA#1	Sigma-Aldrich	TRCN0000090773
pLKO-Col2a1-shRNA#2	Sigma-Aldrich	TRCN0000090775
Software and Algorithms		
DAVID v6.8	Huang *et al.*, 2009	https://david.ncifcrf.gov/
Bowtie v1.1.1	John Hopkins University	http://bowtie-bio.sourceforge.net/index.shtml
Bowtie v2.2.3	John Hopkins University	http://bowtie-bio.sourceforge.net/bowtie2/index.shtml
Samtools v0.1.19	Li *et al.*, 2009	http://www.htslib.org/
Integrative Genomics Viewer (IGV)	Broad Institute	http://software.broadinstitute.org/software/igv/
igvtools v2.3.57	Broad Institute	https://software.broadinstitute.org/software/igv/igvtools
Tophat v2.0.13	John Hopkins University	https://ccb.jhu.edu/software/tophat/index.shtml
cufflinks v2.2.1	Trapnell Lab	http://cole-trapnell-lab.github.io/cufflinks/
HTSeq v0.6.1	Anders *et al.*, 2015	https://github.com/simon-anders/htseq
DESeq2 v1.6.3	Love *et al.*, 2014	http://www.bioconductor.org/packages/release/bioc/html/DESeq2.html
Fiji: ImageJ		https://imagej.net/Fiji
Prism 8	GraphPad Software	https://www.graphpad.com